# A Combined Molecular Dynamics and Diffusion Model of Single Proton Conduction through Gramicidin

Mark F. Schumaker,* Régis Pomès,† and Benoît Roux‡

* Department of Pure and Applied Mathematics, Washington State University, Pullman, Washington 99164-3113 USA; † Theoretical Biology and Biophysics Group, Los Alamos National Laboratory, Los Alamos, New Mexico 87545 USA; and ‡ Groupe de Recherche en Transport Membranaire, Départements de Physique et de Chimie, Université de Montréal, Québec H3C 3J7, Canada

ABSTRACT We develop a model for proton conduction through gramicidin based on the molecular dynamics simulations of Pomès and Roux (*Biophys. J.* 72:A246, 1997). The transport of a single proton through the gramicidin pore is described by a potential of mean force and diffusion coefficient obtained from the molecular dynamics. In addition, the model incorporates the dynamics of a defect in the hydrogen bonding structure of pore waters without an excess proton. Proton entrance and exit were not simulated by the molecular dynamics. The single proton conduction model includes a simple representation of these processes that involves three free parameters. A reasonable value can be chosen for one of these, and the other two can be optimized to yield a good fit to the proton conductance data of Eisenman et al. (1980, *Ann. N.Y. Acad. Sci.* 339:8–20) for pH $\geq$ 1.7. A sensitivity analysis shows the significance of this fit.

## GLOSSARY

Symbols that appear in two or more subsections are given. When uppercase and lowercase symbols are given together, lowercase denotes dimensionless quantities. Species $s$ may represent either H (proton) or d (defect). Roman R denotes either side I or side II of the channel.

### Latin symbols

| | |
|---|---|
| $C_R$ | Bulk concentration on side R (see Fig. 1 *B*) |
| $D^s$ | Effective standard diffusion coefficient for species $s$ (see Eq. 22) |
| $\mathscr{D}^s$ | Diffusion coefficient of dipole moment reaction coordinate (Eq. 17) |
| $\mathscr{D}^i$ | Diffusion coefficient for independently tumbling waters (Appendix A) |
| $\hat{\mathscr{D}}$ | Laplace transform of diffusion coefficient (Eq. 16) |
| $E$ | Electric field in pore (Eq. 23) |
| $e$ | Base of natural logarithms |
| $e_0$ | Elementary electrical charge |
| $G_0$ | Single proton model conductance at symmetrical equilibrium (see Eq. 21) |
| $G_V$ | Chord conductance at potential $V$ |
| $G_{max}$ | Maximum apparent single proton conductance (see above Eq. 21) |
| $K$ | Spring constant |
| $K_M$ | Apparent Michaelis constant (see above Eq. 21) |
| $k$ | Rate of barrier crossing (Eq. 18 and Appendix B) |
| $k_B$ | Boltzmann's constant |
| $I$ | Current through channel (Eq. 21) |
| $L$ | Spatial length of channel (see Fig. 1 *B*) |
| $n^s$ | Net number of waters in pore with dipole moments oriented in $+z$ direction (Eqs. 2 and 7) |
| $n_{max}$ | Number of water molecules in pore (Eq. 5) |
| $T$ | Absolute temperature |
| $t^a$ | Framework model free parameter (see Optimization of Model Parameters in Methods) |
| $t$ | Time |
| $\bar{t}$ | Mean first passage time |
| $V_I$ | Applied transmembrane potential (see Fig. 1 *B*) |
| $z$ | Spatial coordinate coaxial with the pore (see Fig. 1 *B*) |

### Greek symbols

| | |
|---|---|
| $\gamma$ | Friction coefficient (Appendix A) |
| $\zeta$ | Framework model free parameter (see above Eq. 21) |
| $\mu^s$ | Dipole moment reaction coordinate for species $s$ (see Eqs. 3 and 8) |
| $\pm\mu^s_A$ | Maximum extents of dipole moment intervals (see Eqs. 6 and 10) |
| $\mu^w$ | Dipole moment of a water molecule (Eq. 1) |
| $\sigma^s$ | Scaling factor between the orientation and dipole moments for species $s$ |
| $\Phi^s$ | Potential of mean force for species $s$ (see Fig. 2) |
| $\chi^s$ | Orientation moment for species $s$ (see above Eq. 1) |
| $\chi^d_{min}$ | Orientation moment coordinate of $\Phi^d$ potential minimum |
| $\pm\chi^s_A$ | Maximum extent of orientation moment interval (see Fig. 2 and Eqs. 5 and 9) |

*Received for publication 14 February 2000 and in final form 1 September 2000.*

Dr. Pomès' present address is Department of Structural Biology and Biochemistry, Hospital for Sick Children, Toronto, ON M5G 1X8, Canada.

Dr. Roux's present address is Department of Biochemistry and Structural Biology, Weill Medical College of Cornell University, 1300 York Ave., New York, NY 10021.

Address reprint requests to Dr. Mark F. Schumaker, Department of Pure and Applied Mathematics, Washington State University, Pullman, WA 99164. Tel.: 509-335-7273; Fax: 509-335-1188; E-mail: schumaker@wsu.edu.



0006-3495/00/12/2840/18 $2.00

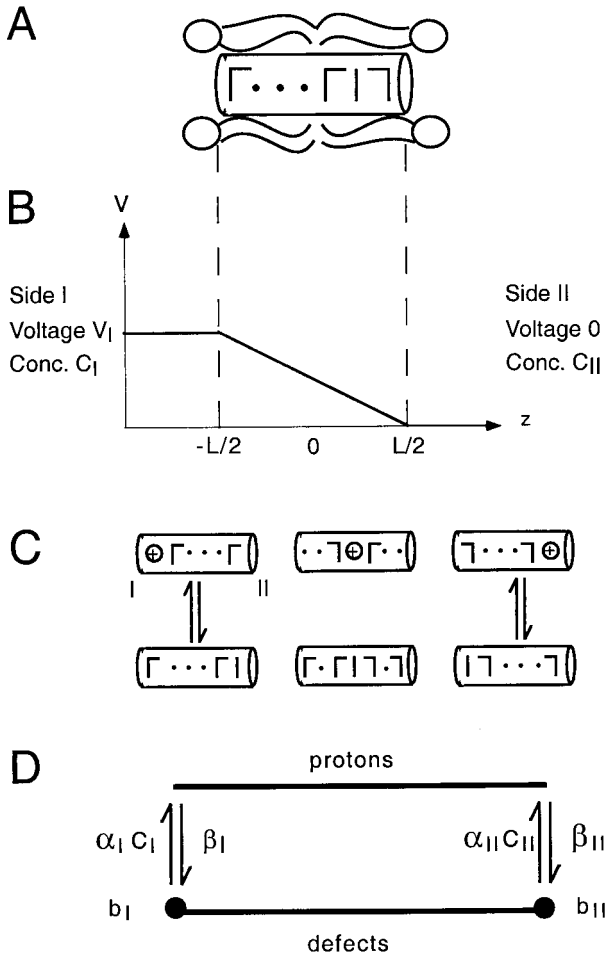


FIGURE 1 (*A*) Orientation of water molecules. Water molecules tend to be oriented so that each shares one hydrogen bond with the channel and two with neighboring waters. The axial component of the water dipole moments may reverse about a water that shares two bonds with the channel. This 2D depiction of hydrogen bonds is stylized; no true asymmetry about the pore axis is implied. (*B*) Applied potential. The single-proton model assumes that the electrical potential, $V$, is a linear function of the coordinate parallel to the pore axis, $z$. Side I refers to the solution on the left, and side II refers to the solution on the right. $V_I$ is the applied electrical potential on side I. $V_{II} = 0$ by convention. (*C*) Hypothetical single-proton conduction mechanism. The top row of cartoons shows a pore with an excess proton. The proton may enter the channel on side I at the upper left. In this cartoon, the orientation of the pore waters favors entrance on side I. As the proton passes through the pore, the hydrogen bond structure of surrounding waters is altered so that water oxygens remain oriented toward the center of excess charge. The bottom row shows a pore in the absence of an excess proton. Water dipole moments flip as a defect in the hydrogen bonding structure diffuses through the column of waters. (*D*) State diagram of the single-proton model. The top segment corresponds to the proton-occupied pore and is parameterized by the coordinate $\mu^H$. The bottom segment corresponds to a defect traversing the central barrier in Fig. 2 *B* and is parameterized by $\mu^d \in [-\mu_C^d, \mu_C^d]$. The endpoints of the bottom segment are the boundary states $b_I$ and $b_{II}$. They correspond to a defect in the boundary regions $\mu_C^d < |\mu^d| < \mu_A^d$.

$\pm\chi_B^d$ Effective electrical coordinates of boundary regions (see Fig. 2 *B*)

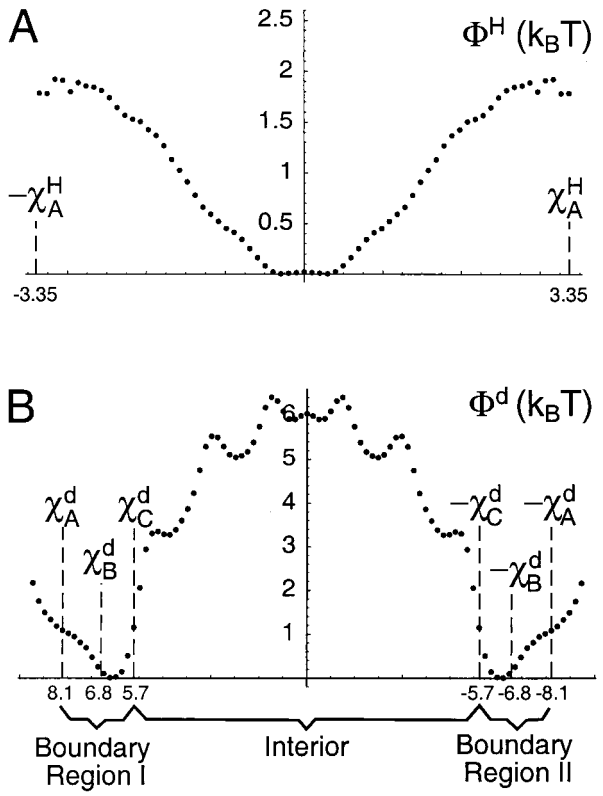


FIGURE 2 Proton and defect potentials of mean force. All energies are given in units of $k_BT$ for $T = 298$ K. (*A*) The ordinate is the proton potential, $\Phi^H$, in $k_BT$, and the abscissa is the orientation moment of the pore contents, $\chi^H$. Dipole moments are obtained by scaling $\mu^H = \sigma^H \chi^H$. (*B*) The ordinate is the defect potential, $\Phi^d$, in $k_BT$, and the abscissa is the orientation moment, $\chi^d$. Protons may enter the channel when defects are in the boundary regions I and II. Shown in the figure are *wide* boundary regions defined by $\chi_A^d = 8.1$, $\chi_B^d = 6.8$, and $\chi_C^d = 5.7$ $e_0$Å. The text also considers *narrow* boundary regions with $\chi_A^d = 8.1$, $\chi_B^d = 7.44$, and $\chi_C^d = 6.9$ $e_0$Å. Boundary regions surround the interior of the defect interval, defined by $-\chi_C^d \le \chi^d \le \chi_C^d$. Dipole moments are obtained by scaling $\mu^d = \sigma^d \chi^d$.

$\pm\chi_C^d$ Maximum extent of interior of defect interval (see Fig. 2 *B*)

$\chi^w$ Orientation moment of a water molecule (Eq. 1)

$\Psi$ Electrical potential energy of pore contents (Eq. 23)

## INTRODUCTION

Proton conduction through gramicidin has gained recent attention because 1) Single-channel currents are large and can be measured over a very wide range of concentrations. The observed conductance has a very prominent shoulder as a function of $[H^+]$ between pH 1 and pH 2 (Eisenman et al., 1980). This observation has been confirmed by Akeson and Deamer (1991), and a similar shoulder has recently been observed in the RR dioxolane gramicidin analog by Cu-

kierman (2000). 2) Experimental evidence suggests that the proton permeation mechanism is qualitatively different from that for other cations (Busath et al., 1998; Phillips et al., 1999). Molecular dynamics simulations suggest that water reorientation may be involved in the rate-limiting steps (Pomès and Roux, 1997, and manuscript in preparation). 3) Proton conduction can be used to probe permeation by other cations (Heinemann and Sigworth, 1989). 4) Proton conduction through gramicidin provides an interesting comparison with other proton channels (DeCoursey and Cherney, 2000). Among the latter are channels that form parts of molecular machines that convert proton gradients into chemical energy by synthesizing ATP (for example, Boyer, 1997) or convert proton gradients into mechanical energy by turning flagellar rotors (for example, Elston and Oster, 1997).

This paper develops a model for proton conduction through gramicidin based on the molecular dynamics simulations of Pomès and Roux (1997 and manuscript in preparation). These simulations incorporate the detailed structure of the channel (Arseniev et al., 1985). Techniques developed to describe the dynamics of this relatively simple molecule may soon be applied to channels of broader biological importance. Nuclear magnetic resonance and x-ray crystallography have recently provided high-resolution structures for several ion channels (Cowan et al., 1992; Ketchem et al., 1993; Doyle et al., 1998; Chang et al., 1998).

A large gap separates the time scales of molecular motions described by molecular dynamics and the time scales required to form meaningful averages of ion permeation events comparable to experimentally observed conductances. In a companion paper (Schumaker et al., 2000b) we develop a *framework model* for ion permeation that bridges the gap. This probabilistic model is designed to combine the results of molecular dynamics with simple assumptions about the proton entrance and exit processes that were not addressed by the simulations. The framework model is based on two coupled Nernst-Planck equations, one describing diffusion of a single proton and the other describing diffusion of a defect in the hydrogen bond structure of pore waters. The interaction between proton permeation and the dynamics of the pore waters can be understood in terms of a state diagram analogous to those encountered in rate theory.

The present paper is chiefly concerned with incorporating the results from molecular dynamics into the framework model and making a detailed comparison with experiment. We discuss the proton and water reorientation potentials of mean force and deconvolute their velocity autocorrelation functions to obtain numerical values for diffusion coefficients. We also verify that a mathematical approximation made by the framework model, the *lumped state approximation*, is accurate when applied to the water reorientation potential of mean force. After incorporating the information from molecular dynamics, the model has three free parameters. These are concerned with proton entrance and exit—processes not addressed by the simulations.

Values for these parameters are obtained from the conductance and conductance ratio data of Eisenman et al. (1980), who present an extensive set of measurements for $pH \geq 1.7$, where we believe single proton conductance dominates. A reasonable value is chosen for one parameter, and the other two are optimized to fit the data. A good fit is obtained, and the resulting model is also compared with two *I–V* curves measured by Decker and Levitt (1988). We also discuss our model in light of the recent experimental results of Phillips et al. (1999) on proton conduction in gramicidin analogs.

## METHODS

### Dipole moment of the gramidicin pore contents

The pore of gramicidin is roughly cylindrical, and consequently an experimentally applied transmembrane potential gives rise to an approximately constant electric field within the pore (Jordan, 1982; Jordan et al., 1989; Roux, 1999). A sketch of the pore geometry is given in Fig. 1 *A*. When the electric field is constant, the component of the pore potential energy due to the applied field depends only on the net charge and the *z* component of the dipole moment of the pore contents (Schumaker et al., 2000b). In part for this reason, we use the *z* component of the dipole moment of the pore contents as the reaction coordinate for the single-proton model.

The reaction coordinate of the molecular dynamics simulation of Pomès and Roux 1997; manuscript in preparation) depends on the *orientation moment* of the polarizable and dissociable PM6 waters (Stillinger and David, 1978; Weber and Stillinger, 1982) occupying the pore. Fig. 2, *A* and *B*, shows the potential of mean force of the pore contents with and without an excess proton, respectively, as a function of the *z* component of the orientation moment. This section describes what the orientation moment is and how it is rescaled to obtain an estimated dipole moment of the water column. We refer to a channel pore without an excess proton as an *empty* pore.

The orientation moment of a single water molecule is the formal dipole moment obtained by assigning oxygen a formal charge of $-2e_0$ and hydrogen a formal charge of $+1e_0$. The OH separation of the model water is $\sim$1 Å, and the H-O-H angle is $\sim$110°. Thus the orientation moment of the PM6 water molecule is $\sim 2 \cos 55° \approx 1.15e_0$ Å. Based on the work of Duca and Jordan (1997; see Results), we use the constant value of 2.4 Debye $= 0.5e_0$ Å for the water dipole moment in both empty and occupied pores. We therefore introduce a scaling factor of $\sigma^{\mathrm{d}} = 0.5/1.15$ between the orientation moment and the estimated water dipole moment.

A water typically forms one hydrogen bond with a pore backbone carbonyl and additional hydrogen bonds with the neighboring waters on either side. This configuration is suggested in Fig. 1, *A* and *C*, although in a highly stylized representation. The water dipole moments are tilted from the $z$ axis by an average angle of $\sim 45°$. We use the value $\chi^w = (1.15 e_0\,\text{Å}) \cos 45° \approx 0.81\, e_0\text{Å}$ for the $z$ component of the water orientation moment. Then the $z$ component of the water dipole moment, $\mu^w$, is given by

$$\mu^w = \sigma^d \chi^w . \tag{1}$$

The reaction coordinate $\mu^d$ of an empty pore is the $z$ component of the dipole moment of the pore waters. $\chi^d$ is the $z$ component of the orientation moment of the pore waters. These coordinates parametrize the progress of a defect in the hydrogen bond structure of the pore waters (Pomès and Roux, manuscript in preparation). Let $n^d$ be the net number of pore waters with dipole moments oriented in the $+z$ direction: the number of waters with $+z$ orientation minus the number with $-z$ orientation. $\mu^d$ and $\chi^d$ can be expressed in terms of $n^d$:

$$\chi^d = n^d \chi^w , \tag{2}$$

$$\mu^d = n^d \mu^w . \tag{3}$$

Then the relationship between the dipole and orientation moments of an empty channel is simply

$$\mu^d = \sigma^d \chi^d . \tag{4}$$

Let $n_{max}$ be the number of pore waters. To define the single file based on simulations, one can either count only those water molecules that can make up to two hydrogen bonds with other water molecules, or count only waters that are confined near the central axis of the channel pore. $n_{max} = 10$ is a consistent choice according to both criteria (Pomès and Roux, 1996). We must have $-n_{max} \le n^d \le n_{max}$. Let $\chi^d_A$ and $\mu^d_A$ be the maximum magnitudes of $\chi^d$ and $\mu^d$, respectively, corresponding to configurations with all waters aligned. We then have $-\chi^d_A \le \chi^d \le \chi^d_A$ and $-\mu^d_A \le \mu^d \le \mu^d_A$, where

$$\chi^d_A = n_{max} \chi^w , \tag{5}$$

$$\mu^d_A = n_{max} \mu^w , \tag{6}$$

and $\mu^d_A = \sigma^d \chi^d_A$. With the value of $\chi^w$ obtained above, we have $\chi^d_A \approx 8.1\, e_0\text{Å}$. In Fig. 2 *B* this value corresponds to the inflection points exterior to the potential minima on either side of the central barrier. Although the range of $\chi^d$ values formally extends to $\pm 9.1\, e_0\text{Å}$, the most extreme values correspond to strained configurations that are probably of little physical importance.

When the pore is occupied by an excess proton, the dipole moment includes a contribution due to the excess charge calculated about the center of the pore, $z = 0$:

$$\chi^H = e_0 z + n^H \chi^w , \tag{7}$$

$$\mu^H = e_0 z + n^H \mu^w , \tag{8}$$

where $n^H$ is the net number of pore waters with dipole moments oriented in the $+z$ direction in the occupied channel. We assume $-n_{max} \le n^H \le n_{max}$. If the pore occupies the interval $-L/2 \le z \le L/2$, it follows that $-\chi^H_A \le \chi^H \le \chi^H_A$ and $-\mu^H_A \le \mu^H \le \mu^H_A$, where

$$\chi^H_A = e_0 L/2 - n_{max} \chi^w , \tag{9}$$

$$\mu^H_A = e_0 L/2 - n_{max} \mu^w . \tag{10}$$

In the occupied channel, the idealized state of maximum dipole moment corresponds to the excess charge at the extreme coordinate $z = L/2$, with $n_{max}$ pore water dipole moments aligned in the $-z$ direction (see the upper right cartoon of Fig. 1 *C*). In this way, the partial negative charges carried by water oxygens are closest to the center of positive charge.

Combining Eqs. 5 and 9 and Eqs. 6 and 10, we have

$$\chi^d_A + \chi^H_A = e_0 L/2 = \mu^d_A + \mu^H_A . \tag{11}$$

From the molecular dynamics, $\chi^H_A = 3.35\ e_0\text{Å}$; then using $\chi^d_A = 8.1\, e_0\text{Å}$, we obtain $L = 22.9$ Å, $\sim 2$ Å shorter than the physical length of the pore. This discrepancy may be explained, at least in part, by the procedure used to simulate the channel occupied by an excess proton. In these simulations, the pore is occupied by 10 PM6 water molecules, and there are also several TIP3P waters clustered about the channel entrances at either end. The TIP3P waters cannot form hydrogen bonds. The closest that the excess proton can approach the channel entrances corresponds to hydronium-like ($H_3O^+$) configurations on the outermost PM6 waters. If the TIP3P waters were able to host hydrogen bonds, there would be $O_2H_5^+$ ions between the PM6 and TIP3P waters. Therefore, the value of $\chi^H_A$ obtained from the simulations may be slightly low, and, as a result, the effective length of the simulated channel may be slightly shorter than the pore of gramicidin.

Finally, we will obtain a scaling factor relating the molecular dynamics reaction coordinate $\chi^H$ and the pore dipole moment $\mu^H$. We make the simplifying assumption that when the excess proton is located at coordinate $z$, all water dipole moments will be oriented away from it, with water oxygens aligned toward the excess positive charge. Then $n^H$ will be a linear function of $z$. Put

$$n^H = -(2/L) n_{max} z , \tag{12}$$

so that when $z = L/2$ (the proton is at the entrance on side II), $n^H = -n_{max}$. Substituting Eq. 12 into Eqs. 7 and 8, and then dividing, we have

$$\mu^H = \sigma^H \chi^H , \tag{13}$$

where

$$\sigma^{H} = (e_0 L - 2n_{max}\mu^{w})/(e_0 L - 2n_{max}\chi^{w}) . \qquad (14)$$

## Diffusion coefficients

Diffusion coefficients were calculated following the method of Crouzy et al. (1994) and Woolf and Roux (1994), based on the Generalized Langevin equation (Berne et al., 1988; Straub and Berne, 1988; Berne and Pecora, 1976):

$$m\ddot{\mu} + \int_0^t M(t-\tau)\dot{\mu}(\tau)d\tau + K\mu = F(t) , \qquad (15)$$

where $\mu$ is the reaction coordinate (the $z$ component of the dipole moment of the pore content), $m$ is a reduced mass, $K$ is a spring constant, $M$ is the memory kernel (a generalized friction coefficient), and a dot denotes the derivative with respect to time. $F(t)$ represents the influence of degrees of freedom orthogonal to the reaction coordinate. Assuming that these other degrees of freedom relax on much shorter time scales than the reaction coordinate, $F(t)$ is modeled as a random process.

If Eq. 15 is multiplied by $\dot{\mu}(0)$ and an ensemble average is taken, an equation is obtained for the velocity autocorrelation function of $\mu$. The result is then Laplace transformed, and the Einstein relation is applied to find a formula for the Laplace transform of the diffusion coefficient (Crouzy et al., 1994; Woolf and Roux, 1994):

$$\hat{\mathcal{D}}(s) = \frac{-\hat{c}(s)\langle\mu^2\rangle\langle\dot{\mu}^2\rangle}{\hat{c}(s)[s\langle\mu^2\rangle + \langle\dot{\mu}^2\rangle/s] - \langle\mu^2\rangle\langle\dot{\mu}^2\rangle} . \qquad (16)$$

In this expression, $\hat{c}(s)$ is the Laplace transform of the velocity autocorrelation function $c(t) = \langle\dot{\mu}(t)\dot{\mu}(0)\rangle$, and $\langle\ldots\rangle$ denotes ensemble average. The diffusion coefficient is obtained as the limit

$$\mathcal{D} = \lim_{s\to 0} \hat{\mathcal{D}}(s) . \qquad (17)$$

For simplicity, we have assumed that the proton and defect diffusion coefficients are constant, independent of the value of their reaction coordinates. In both cases, $c(t)$ was computed from molecular dynamics simulations at 0.5-fs intervals for times in the range $0 < t < 0.5$ ps. Fig. 3 *A* shows the normalized proton velocity autocorrelation function $\langle\chi^{H}(t)\chi^{H}(0)\rangle$ for the proton reaction coordinate held near $\chi^{H} = 2.99$ $e_0$Å by an umbrella potential. Values of the proton orientation moment are scaled to the dipole moment by $\mu^{H} = \sigma^{H}\chi^{H}$, as described in the previous section. Fig. 4 *A* shows $\hat{\mathcal{D}}^{H}$ as a function of $s$. Parabolic extrapolation of $\hat{\mathcal{D}}^{H}$ from the interval $10 < s < 40$ gives an estimate $\mathcal{D}^{H} = 3.52 \times (\sigma^{H})^2$ $(e_0$ Å$)^2$ ps$^{-1}$. The smooth behavior of $\hat{\mathcal{D}}^{H}$ at high values of $s$ becomes corrupted for $s < 10$ corresponding to times $t > 0.1$ ps. This may reflect other processes influencing the transport of protons on longer time scales, for example, interactions between proton motion and rearrangement of hydrogen bonds.

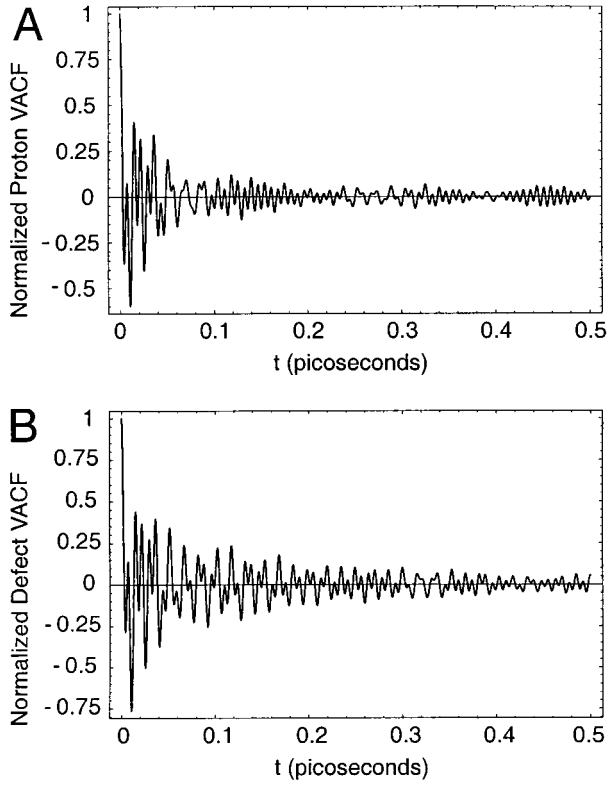


FIGURE 3 Velocity autocorrelation functions. (*A*) The normalized proton velocity autocorrelation function $\langle\chi^{H}(t)\chi^{H}(0)\rangle$ for the reaction coordinate held near $\chi^{H} = 2.99$ $e_0$Å by an umbrella potential. The unnormalized amplitude is $\langle\chi^{H}(t)^2\rangle = 7346.6$ $(e_0$ Å$)^2$ ps$^{-1}$. (*B*) The normalized defect velocity autocorrelation function for the reaction coordinate held near $\chi^{d} = -0.104$ $e_0$Å by an umbrella potential. The unnormalized amplitude is $\langle\chi^{d}(t)^2\rangle = 5270.8$ $(e_0$ Å$)^2$ ps$^{-1}$.

Similarly, the defect diffusion coefficient was estimated from the defect reaction coordinate held near $\chi^{d} = -0.104$ $e_0$Å by an umbrella potential. Values of the defect dipole moment are given by $\mu^{d} = \sigma^{d}\chi^{d}$. Fig. 3 *B* shows the normalized defect velocity autocorrelation function. Fig. 4 *B* shows $\hat{\mathcal{D}}^{d}$ as a function of $s$. Parabolic extrapolation of $\hat{\mathcal{D}}^{d}$ from the interval $4 < s < 10$ gives an estimate $\mathcal{D}^{d} = 1.08 \times (\sigma^{d})^2$ $(e_0$ Å$)^2$ ps$^{-1}$. Values of $\hat{\mathcal{D}}^{d}$ become corrupted for $s < 3$ corresponding to times $t > 0.33$ ps; this reflects the finite interval of times for which $c(t)$ was computed.

## The lumped state approximation

The framework model lumps the boundary regions of the defect potential of mean force, shown in Fig. 2 *B*, into discrete boundary states. These are represented by the filled endpoints of the bottom segment of the state diagram shown by Fig. 1 *D*. The weights of these boundary states are

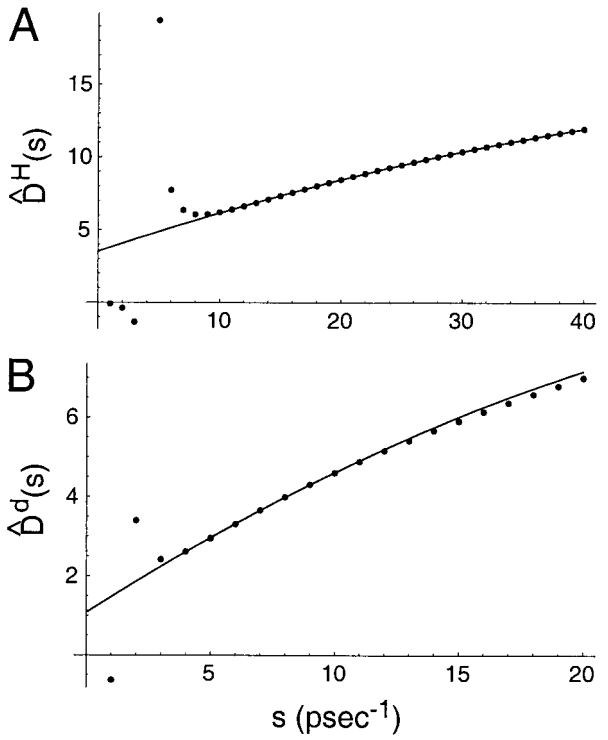


FIGURE 4 Estimates of diffusion coefficients. In each figure, the numerical estimate of the Laplace transform of the diffusion coefficient, $\hat{\mathcal{D}}$, is shown as a function of the transform parameter $s$. (*A*) Values of $\hat{\mathcal{D}}^H(s)$. Parabolic extrapolation to the ordinate gives the estimated proton diffusion coefficient of $\mathcal{D}^H = 3.52 \times (\sigma^H)^2$ $(e_0$ Å$)^2$ ps$^{-1}$. The Laplace transform is shown for $\sigma^H = 1$. (*B*) Values of $\hat{\mathcal{D}}^d(s)$. The estimated defect diffusion coefficient is $\mathcal{D}^d = 1.08 \times (\sigma^d)^2$ $(e_0$ Å$)^2$ ps$^{-1}$. The transform is shown for $\sigma^d = 1$.

carefully adjusted to give the integral over the Boltzmann distribution under the conditions of a symmetrical equilibrium (Schumaker et al., 2000b). This *lumped state approximation* (LSA) makes it possible to solve the framework model analytically. However, the boundary states act electrically like points with electrical coordinates $\pm\chi_B^d$, where $\chi_B^d$ is a free parameter of the framework model. The value of $\chi_B^d$ is chosen to give the best possible representation of the mean first passage time (MFPT) over the defect potential barrier as a function of the applied potential $V_I$.

To determine the best possible representation of the MFPT, consider a diffusion process that does not depend on the lumped state approximation. This latter process is defined on the interval $[-\chi_A^d, \chi_A^d]$ of the potential profile shown in Fig. 2 *B*. The process starts at $\chi^d = -\chi_{min}^d = -6.5$ $e_0$Å, a minimum of $\Phi^d$, with a reflecting barrier at $\chi^d = -\chi_A^d$. The mean first passage time to $\chi^d = \chi_{min}^d$ is then calculated as described in Appendix B. Because the MFPT found in this way is the standard for comparison, we call it the *exact* MFPT. An analytical formula can also be obtained for LSA MFPTs, as will be described by Mapes and Schumaker (manuscript submitted for publication). These mean times correspond to a process that starts at the lumped state at $\chi^d = -\chi_C^d$. The exact mean first passage time to the lumped state at $\chi_C^d$ is then given. Values of the electrical coordinate for the lumped states, $\chi_B^d$, are chosen so that LSA MFPTs approximate the exact values well over the range of applied potentials, $-200$ mV $\leq V_I \leq 200$ mV.

Fig. 5 *A* compares the LSA MFPTs over the central barrier shown in Fig. 2 *B* with the exact MFPTs. The logarithm of the MFPTs is shown as a function of the applied potential $V_I$. When $V_I > 0$, the potential energy of the well centered at $\chi^d = -\chi_{min}^d$ is increased relative to the energy of the well at $\chi_{min}^d$, reducing the MFPT. To test the sensitivity of our results to the value of $\chi_C^d$, MFPTs for the LSA are calculated for both *wide* and *narrow* boundary regions. The wide boundary regions are shown in Fig. 2 *B*

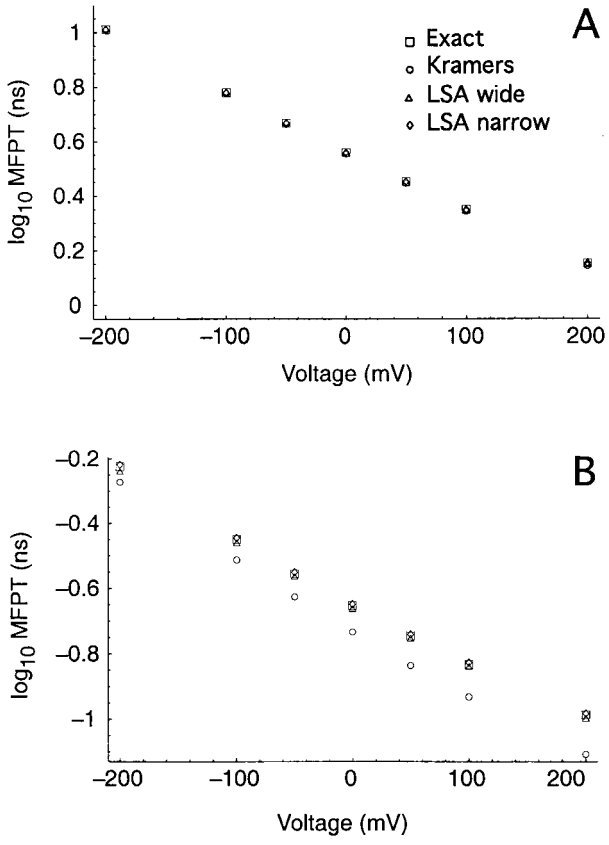


FIGURE 5 Logarithm of the mean first passage time over the defect potential central barrier plotted as a function of the applied electrical potential. Squares and circles give estimates of the mean first passage time that apply to the potential defined in the full interval between $\pm\chi_A^d$. Squares give the exact mean first passage between the potential minima, with reflecting boundary conditions at $\pm\chi_A^d$. Circles give the Kramers approximation to the mean first passage time. Triangles give mean first passage times, using boundary states with $\chi_C^d = 5.7$ $e_0$Å. Diamonds give times using boundary states with $\chi_C^d = 6.9$ $e_0$Å. (*A*) Defect potential given by molecular dynamics. (*B*) Defect potential rescaled so that the height of the central barrier is $4k_BT$ lower than that given by molecular dynamics.

and have $\chi_C^d = 5.7$, $\chi_B^d = 6.8$, and $\chi_A^d = 8.1\ e_0$Å. The narrow boundary regions have half the width of the wide regions, with $\chi_C^d = 6.9$, $\chi_B^d = 7.44\ e_0$Å, and the same value of $\chi_A^d$. Also shown in Fig. 5 *A* are MFPTs estimated by using Kramers' escape theory (e.g., Risken, 1989). The integrals in the Kramers formula are calculated numerically so that a robust estimate of the MFPT is obtained, even though the crest of the central barrier in Fig. 2 *B* has a complex shape; this is described in Appendix B. As shown by Fig. 5 *A*, MFPTs obtained by all four methods are in very good agreement over the full range of applied potentials considered.

The sensitivity analysis presented in the Results depends on the LSA remaining accurate for a range of barrier heights. In one case, the amplitude of the potential profile shown in Fig. 2 *B* is reduced by $4k_BT$, leaving a barrier that is little more than $2k_BT$ high in the absence of an applied potential. Fig. 5 *B* shows how the LSA MFPTs then compare with the other MFPT values. Both sets of LSA MFPTs remain in good agreement with the exact values. However, estimates of the MFPT obtained from the Kramers formula diverge from the other values as $V_I$ increases. This is not surprising, because Kramers' theory is an asymptotic approximation that is accurate when potential barriers are higher than $\sim 4k_BT$ (Cooper et al., 1985, 1988). However, when $V_I = 200$ mV, the height of the potential barrier as seen by a diffuser beginning on side I is less than $1k_BT$.

Fig. 5 shows that the logarithm of the mean first passage time is approximately a linear function of $V_I$. An interesting comparison can be made between linear least-squares fits to the points in the figure and the expected expression in the limit of high potential barriers. According to Kramers' theory, the rate $k$ of barrier crossing in the latter limit has the form

$$k = A\exp[-\Delta W^d/k_BT], \tag{18}$$

where $\Delta W^d$ is the height of the total defect potential barrier and $A$ is a constant. The total potential, $W^d$, is the sum of the potential of mean force, $\Phi^d$, and the electrical potential energy, $\Psi^d$ (Schumaker et al., 2000a). The mean first passage time corresponding to rate $k$ is $1/k$. The height, $\Delta W^d$, depends on the applied potential according to

$$\Delta W^d = \Delta W_0^d - fe_0V_I, \tag{19}$$

where $\Delta W_0^d$ is the height in the absence of an applied electrical potential and $f$ is the fraction of the electrical potential drop between the maximum and minima of $\Phi^d$. To be precise, put $f = \sigma^d\chi_{min}^d/(e_0L)$, where $\chi_{min}^d = 6.5\ e_0$Å is the coordinate of the defect potential minimum and $e_0L = 22.9\ e_0$Å is the total potential drop associated with the passage of a proton across the membrane (see Eq. 11). The predicted slope of $\log_{10}$ (mean first passage time) as a function of $V_I$ is then $-m$, where

$$m = (\log_{10} e)\, fe_0/(1000k_BT), \tag{20}$$

and where $e$ is the base of the natural logarithms, $e_0$ is the elementary electrical charge, and the factor of 1000 is due to measuring $V_I$ in mV.

Using the value of $\sigma^d$ described above (in Dipole Moment of the Gramicidin Pore Contents), we obtain, from Eq. 20, $m = 0.00211$. In comparison, linear least-squares fits through each of the four sets of values in Fig. 5 *A* give slopes in the range $0.00214 \le m \le 0.00216$, close to the limiting value. However, linear least-squares fits through the exact and LSA sets in Fig. 5 *B* give $0.00189 \le m \le 0.00191$. For the $\Delta W_0^d \approx 2k_BT$ potential barrier used to generate the latter figure, the LSA gives a softened dependence of mean first passage time on the applied field, which is similar to the exact result. In contrast, the slope obtained from the Kramers' estimates in Fig. 5 *B* gives $m = 0.00209$.

## Optimization of model parameters

The framework model of proton conduction (Schumaker et al., 2000b) has three free parameters: $\zeta$, $t^a$, and $\chi_C^d$. $\zeta$ depends on the absolute free energy difference between the proton and defect potentials of mean force, and $t^a$ controls the rate of proton exit from the channel; together $\zeta$ and $t^a$ control the rate of proton entrance and exit. $\chi_C^d$ determines the width of the boundary regions of the defect potential profile. These are defined as regions within which there may be a defect in the hydrogen bond structure of waters when a proton enters or leaves the pore (see Fig. 2 *B*).

Initial estimates of $\zeta$ and $t^a$ are based on subjective estimates of the Michaelis constant, $K_M$, and the maximum conductance, $G_{max}$, associated with entry of the first proton into the gramicidin channel. $K_M$ and $G_{max}$ are assumed to be associated with the lower leg of rising conductance in the data of Eisenman et al. (1980), which is measured at symmetrical pH and a transmembrane potential of 50 mV (see Fig. 7 *A*). The estimated values are $K_M = 0.005$ M and $G_{max} = 24$ pS.

We use these estimates to determine values of $X$ and $Y$ in the formula for $G_0$, the conductance at symmetrical concentrations and zero transmembrane potential (Schumaker et al., 2000b):

$$G_0 = \left.\frac{\partial I}{\partial V_I}\right|_0 = \frac{e_0^2}{k_BT}\frac{C}{X + CY + C^2Z}. \tag{21}$$

In this formula, $I$ is the proton current and $V_I$ is the transmembrane potential. The subscript 0 refers to the derivative evaluated at the equilibrium state with symmetrical concentrations $C_I = C_{II} = C$ and $V_I = 0$. The coefficients $X$, $Y$, and $Z$ depend on the three free parameters in the following way: $X = X(t^a, \zeta)$, $Y = Y(t^a, \chi_C^d)$, and $Z = Z(\zeta, \chi_C^d)$.

Assuming a fixed value of $\chi_C^d$, the estimates of $X$ and $Y$ determine initial values of $t^a$ and $\zeta$. This is used as a starting point for local least-squares minimization of the model against the combined data in Fig. 7, *A* and *B*, for pH $\ge$ 1.7.

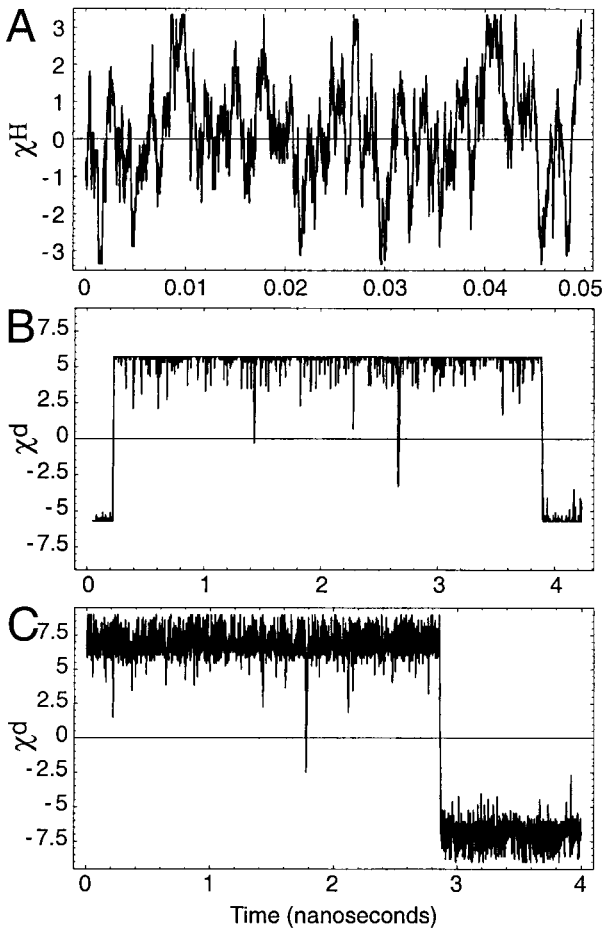


FIGURE 6 Single-proton model trajectories. Trajectories for *A* and *B* are obtained by simulating a random walk approximating the single-proton model for $\chi_C^d = 5.7$ and $\chi_A^d = 9.1e_0$ Å, $C_I = C_{II} = 0.01$ M, and $V_I = 0$. (*A*) A proton trajectory. (*B*) A defect trajectory. Occupation of the boundary states is indicated at $\chi_C^d = \pm 5.7\ e_0$Å. (*C*) Defect trajectories diffusing in the full interval of reaction coordinate defined by the molecular dynamics simulations.

$t^a$ and $\zeta$ are varied to minimize the sum of unweighted differences between the $\log_{10}G_{50}$ data (Fig. 7 *A*) and the model plus twice the sum of the unweighted differences between the conductance ratio data (Fig. 7 *B*) and the model. We consider two different values of the third parameter controlling the width of the boundary regions: $\chi_C^d = 5.7\ e_0$Å, giving wide boundary regions, and $\chi_C^d = 6.9\ e_0$Å, giving narrow boundary regions. These are used to generate the fits shown in Fig. 7, *A* and *B*.

## RESULTS

### Molecular dynamics simulations

Pomès and Roux (manuscript in preparation) have simulated the dynamics of proton conduction through gramicidin. The orientation of the channel pore in the membrane is sketched in Fig. 1 *A*. The packing of the pore contents in several configurations is represented in simplified form by Fig. 1 *C*. In one set of simulations the pore includes an excess proton; these are represented by the top row of the figure. The water oxygens tend to be oriented toward the center of excess charge. The resulting water dipole moments partially offset the contribution of the excess proton to the total pore dipole moment.

In a second set of simulations, there is no excess proton. These are represented by the bottom row of Fig. 1 *C*. It is energetically favorable for interior pore waters to share one hydrogen bond with the channel and two others with the adjacent water molecules. In this way they tend to have their dipole moments aligned with similar *z* components. However, pore waters near the channel entrances tend to be less ordered. As a result, there is often a localized disorder in the packing structure of the pore waters near the entrance, centered on a water molecule that shares two hydrogen bonds with the channel. This disordered region may diffuse from one end of the pore to the other, reversing the dipole moments of the pore waters.

#### *Potentials of mean force*

Fig. 2 shows the potentials of mean force plotted as a function of the orientation moment $\chi^H$ or $\chi^d$, the reaction coordinate of the simulations. In Methods, we discuss how these orientation moments can be scaled to obtain estimated components of the dipole moment of the pore contents parallel to the pore axis: $\mu^d = \sigma^d\chi^d$ and $\mu^H = \sigma^H\chi^H$. Dipole moments are calculated with respect to the center of the pore, at $z = 0$. According to the notation introduced in Fig. 2, axial components of the proton dipole moments vary over the range $-\mu_A^H \le \mu^H \le \mu_A^H$, and defect components vary over $-\mu_A^d \le \mu^d \le \mu_A^d$. The total interval of dipole moment spanned by the two potentials is 22.9 $e_0$Å, corresponding to an elementary charge passing through the length of a pore 22.9 Å long. This is somewhat shorter than the physical length of the gramicidin pore, which is ~25 Å. A possible explanation for this discrepancy is offered in Methods.

The scaling factor $\sigma^d$ is calculated by assuming that the average dipole moment of a water molecule in the pore is 2.4 Debye. By comparison, Duca and Jordan (1997) have estimated effective average dipole moments of water molecules in a simulated polyglycine analog of gramicidin. In their simulations with all groups polarizable, the average water dipole moment in an empty pore was found to be ~2.3 Debye. In a pore occupied by a single $Na^+$ or $Cs^+$ ion, this moment depends on the proximity of the water to the ion and varies between 2.3 Debye far from the ion (e.g., fifth nearest neighbors) to 3.0 Debye next to the ion.

The value of $\mu_A^d$ used corresponds to the *z* component of the dipole moment of a column of 10 aligned water molecules, each tilted at an angle of 45° from the pore axis, consistent with the conformation of waters in the pore.

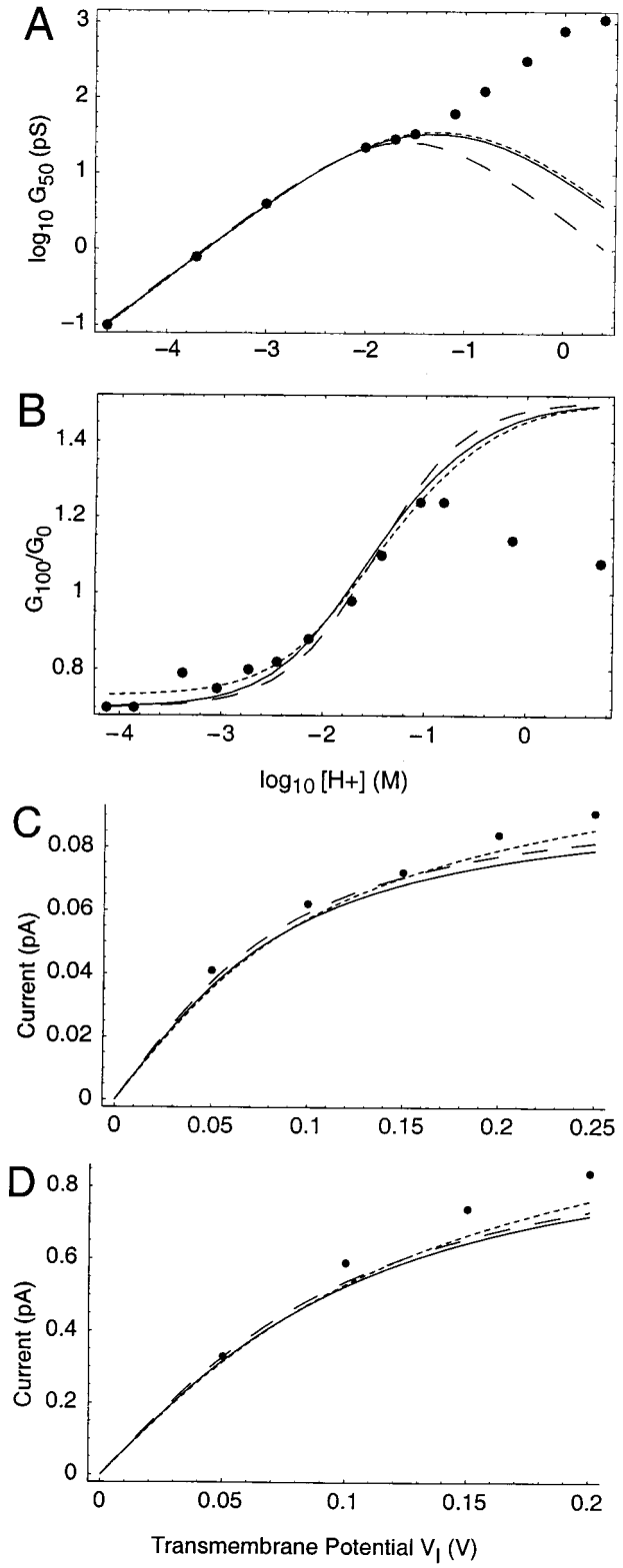


FIGURE 7 Comparisons between the framework model and experimental data. Circles are the data of Eisenman et al. (1980). Curves show framework model fits to data. Fits are made optimizing the values of $t^a$ and $\zeta$, parameters that control the rate of proton entry and exit. Solid curves show fits using molecular dynamics estimates of potentials of mean force and diffusion coefficients, and the *wide* boundary regions shown in Fig. 2 *B*; optimized values are $t^a = 23.5$ ns and $\zeta = 3.60$. Long-dashed curves show fits using a defect potential of mean force scaled to an amplitude $2k_BT$ higher than that given by molecular dynamics; the proton potential of mean force and all diffusion coefficients are those given by molecular dynamics. Optimized values are $t^a = 16.5$ ns and $\zeta = 3.53$. Short-dashed curves show fits using molecular dynamics estimates of potentials and diffusion coefficients and *narrow* boundary regions. Optimized values are $t^a = 21.6$ ns and $\zeta = 2.23$. (*A*) Fits to conductance measured at 50 mV applied potential. (*B*) Fits to conductance ratios. The experimental data are conductances measured at 100 mV divided by estimated conductances at 0 mV. (*C*) Comparison between framework model fits to data of Eisenman et al. and the experimental *I–V* curve of Decker and Levitt (1988) at pH 3.75. (*D*) Comparison with Decker and Levitt *I–V* curve at pH 2.75.

Calculation of the scaling factor $\sigma^H$ also assumes that the center of excess charge in the occupied pore separates two subcolumns of water molecules, both with dipole moments aligned so that oxygens are brought close to the excess proton. Details of these calculations are presented in Methods.

The proton potential is a shallow well. As a consequence, charge density corresponding to an excess proton concentrates near the center of the pore. The defect potential has two minima separated by an $\sim 6k_BT$ barrier. Thus the defect concentrates in regions near the channel entrances, on either side of the central barrier. The fine structure of the defect potential is due to both the periodicity of the gramicidin helix and the energetics of breaking hydrogen bonds between the single-file water molecules. The absolute free energy difference between the proton and defect potentials is not known.

Ideally, the potential of mean force should include electrostatic interactions with the membrane and bulk electrolyte (Roux, 1999). Instead, the potentials $\Phi^H$ and $\Phi^d$ depend only on the channel, pore waters, and several additional waters outside the channel entrance. Below, we will present a sensitivity analysis showing how our conclusions change as we perturb the defect barrier height and diffusion coefficient.

### *Diffusion coefficients*

Diffusion coefficients of protons and defects simulated by molecular dynamics were calculated by the Laplace Transform method (Woolf and Roux, 1994; Crouzy et al., 1994), as described in the Methods. We obtained $\mathcal{D}^H = 3.52 \times (\sigma^H)^2\ (e_0\text{Å})^2\ \text{ps}^{-1}$ and $\mathcal{D}^d = 1.08 \times (\sigma^d)^2\ (e_0\text{Å})^2\ \text{ps}^{-1} \approx 0.20\ (e_0\text{Å})^2\ \text{ps}^{-1}$. The defect value can be compared with a simple estimate of the dipole diffusion coefficient $\mathcal{D}^i$ for a model of 10 independently tumbling water molecules. In Appendix A we obtain $\mathcal{D}^i = 0.36\ (e_0\ \text{Å})^2\ \text{ps}^{-1}$, comparable to the values of $\mathcal{D}^d$ given above.

The value of $\mathcal{D}^H$ can be associated with a standard diffusion coefficient in the following way. Consider a proton starting at one channel entrance and diffusing to the other entrance. In the absence of a potential and assuming a

reflecting boundary at the starting point, the mean first passage time to reach the goal is $\bar{t} = (2\mu_A^H)^2/(2\mathcal{D}^H)$. The corresponding mean first passage time to diffuse the physical length, $L$, of the pore with a standard diffusion coefficient $D^H$ is $\bar{t} = L^2/(2D^H)$. Equating these two expressions, we obtain

$$D^H = \mathcal{D}^H L^2/(2\mu_A^H)^2 . \quad (22)$$

Since $\mu_A^H = \sigma^H \chi_A^H$, factors of $\sigma^H$ cancel in this formula. Using the value of $\chi_A^H = 3.35\ e_0$Å from the molecular dynamics and channel length $L = 22.9$ Å, we obtain $D^H \approx 41$ Å$^2$ ps$^{-1}$. This is ~40 times the diffusion coefficient of protons in water, $9.3 \times 10^{-5}$ cm$^2$ s$^{-1}$ = 0.93 Å$^2$ ps$^{-1}$ (Hille, 1992), but only about twice as great as the diffusion coefficient of protons in ice (Eisenberg and Kauzmann, 1969).

The Laplace Transform method of estimating the diffusion coefficient requires extrapolation from a smooth curve, which is determined by an analysis over short time scales. In the case of Fig. 4 *A*, extrapolations are made from values of $s$ corresponding to time scales of ~0.1 ps. Mechanisms operating on longer time scales, such as movement of defects in the water chain, may decrease the effective diffusion coefficient.

## Single-proton conduction model

### *Hypothetical conduction mechanism*

We will construct a kinetic model based on the assumption that protons can only enter the channel under the energetically favorable circumstance that the net dipole moment of the pore contents is pointing away from the proton. The results obtained from the simulations then suggest a mechanism of proton conduction through gramicidin.

The geometry of the pore between aqueous solutions on sides I and II is indicated by Fig. 1 *A*. Sides I and II are also indicated for the upper left cartoon in Fig. 1 *C*. As suggested by Fig. 1 *C*, proton entry into the channel from side I would be facilitated by waters lined up to present a partial negative charge at the channel entrance. As the proton passes through the channel, waters remain oriented to the center of excess charge. When the proton escapes the dipoles remain nearly aligned. A defect must then propagate through the pore to restore the original orientation of waters in the channel. An elementary charge is transferred from side I to side II when the channel cycles once around the diagram clockwise.

The lower middle cartoon in Fig. 1 *C* depicts the defect separating two oppositely aligned columns of water. The dipole moments of both columns point toward the defect, giving it a partial positive charge. This is the nature of the defect most commonly encountered in the simulations. It is called *entrance-initiated* by Phillips et al. (1999), because it originates near the channel entrance opposite the exiting proton. Alternatively, the dipole moments of the two partial columns may point away from the defect, giving it a partial negative charge (an *exit-initiated* defect). The mathematical formulation of the single-proton model does not depend on this choice. Our use of the word "*defect*" here is slightly different from that encountered in reference to Bjerrum L or D defects (for example, Eisenberg and Kauzmann, 1969). In this latter case, a defect refers to an interruption of the hydrogen bond chain. The terminology of Phillips et al. has the advantage of avoiding confusion, because an entrance-initiated defect is likely to propagate through the formation of transient Bjerrum L defects (Pomès, 1999), which are sometimes referred to as *negative* defects.

### *Applied transmembrane potential*

Fig. 1 *B* shows the electrical potential, $V(z)$, due to a voltage difference, $V_I$, between the two sides of the membrane. Suppose $V_I > 0$. In the top row of Fig. 1 *C*, the field pushes the proton toward side II. However, the dipole moment of the pore contents changes sign once the proton leaves the channel, and so the electric field then tends to reverse the orientation of the waters, now pushing the defect from side I to side II. A positive potential on side I favors clockwise cycling around the diagram.

For the relatively uniform cylindrical geometry of the gramicidin pore, the applied electrical potential is well approximated as decreasing linearly across the length of the pore (Jordan, 1982; Jordan et al., 1989; Roux, 1999). In this case, the electrical potential energy of the pore contents, $\Psi$, depends only on its net charge and dipole moment (Schumaker et al., 2000b). The energy is given by

$$\Psi = qV_I/2 - \mu E , \quad (23)$$

where $q$ is the net charge of the pore contents, $\mu$ is the dipole moment calculated about $z = 0$, and $E = V_I/L$ is the constant electric field. For simplicity, we ignore the feathering of the electric field that occurs at the channel entrances in the calculations of Jordan and Roux.

Proton transport through the channel corresponds to an elementary charge moving through the thickness of the membrane. This combination has units of dipole moment and can be associated with dipole moment changes due to diffusion across the proton and defect segments of the state diagram in Fig. 1 *D*. The electrical potential energy drop corresponding to ion or defect translocation through the pore is proportional to the change in pore dipole moment. This total change is $2\mu_A^H \approx 15.86\ e_0$Å in the case of proton translocation and $2\mu_A^d \approx 7.04\ e_0$Å in the case of defect translocation. Thus, ~69% of the applied potential drop drives proton translocation, and the rest drives the defects.

### *Framework model*

Schumaker et al. (2000b) have constructed a *framework* model for single-proton conduction through gramicidin

based on the mechanism of Fig. 1 *C*. The word "*framework*" refers to the model's design, which incorporates the results of the molecular dynamics simulations. Mathematically, it has the form of a pair of Nernst-Planck equations coupled through their boundary conditions. Nernst-Planck equations are the first integrals of Smoluchowski equations, which model diffusion in the presence of systematic forces.

A state diagram for the model is presented in Fig. 1 *D*. The top horizontal line segment represents the possible proton states corresponding to the top row of Fig. 1 *C*. The bottom horizontal line segment corresponds to the possible defect states corresponding to the bottom row of Fig. 1 *C*. Proton entrance and exit were not simulated by the molecular dynamics. The single-proton model incorporates a very simple representation of these processes.

### *Lumped state approximation of boundary regions*

Define boundary regions on either side of the defect segment as regions receptive to protons entering from the appropriate side. For example, protons may enter the channel from side I in Fig. 1 *D* if the defect dipole moment is in boundary region I of Fig. 2 *B*. Mathematically, the boundary regions are lumped as endpoints of the defect segment of the state diagram. These endpoints are the boundary states $b_I$ and $b_{II}$ of Fig. 1 *D*. Proton entrance occurs directly from the boundary states. Schumaker et al. (2000b) show how boundary conditions corresponding to the lumped state approximation are constructed.

Consider the state diagram of Fig. 1 *D*. Proton entrances into the pore from side I occur with rate $Q_I^b \alpha_I C_I$, where $Q_I^b$ is the probability that the boundary state $b_I$ is occupied and $\alpha_I C_I$ is the entrance rate of protons on side I. $C_I$ is the concentration of the excess protons on side I, and $\alpha_I$ is a second-order rate constant. A similar expression holds on side II. The rates of transitions from the proton interval to the boundary states are proportional to the proton probability density at the endpoints of the proton interval. All transitions satisfy detailed balance at equilibrium.

Through the boundary conditions on the Nernst-Planck equations, it is possible to adjust the weight of the boundary states $b_I$ and $b_{II}$ to be proportional to an integral of the Boltzmann factor, $\exp[-\Phi^d(\mu^d)/k_B T]$, over the corresponding boundary regions of the $\mu^d$ axis. Here, $\Phi^d$ is the defect potential of mean force shown in Fig. 2 *B*. As a result, the boundary states give the appropriate description of thermodynamic equilibrium when the transmembrane electrical potential difference is zero.

One limitation of the lumped state approximation of the boundary regions is that the boundary states must act electrically like points. Their electrical coordinates are adjustable parameters of the theory and are chosen to give the best comparison with the exact mean first passage times over the defect barrier. In Methods we compare estimates of the mean first passage time for diffusion over the defect potential barrier as a function of applied potential. This analysis shows that the lumped state approximation accurately models the dependence of mean first passage time on applied potential.

### *Single-proton trajectories*

The framework model is constructed as the limit of a sequence of random walks (Schumaker et al., 2000b). The sequence of random walks is indexed by an integer $n$, denoting the number of states into which the proton and defect segments are divided. Transition probabilities between the states are a function of $n$, and the framework model is obtained in the limit $n \to \infty$. Numerical simulations suggest that transport described by the random walks accurately simulates the limiting diffusion process for moderate values of $n$. Here we use the random walks for $n = 57$ to illustrate ion trajectories underlying the framework model. In particular, we illustrate the boundary behavior of their trajectories.

In Fig. 6 *A* a short 50-ps segment of a proton trajectory is shown. Proton escape is not limited by the shallow potential energy well of the proton potential of mean force, but rather by the boundary conditions. Fig. 6 *B* shows a trajectory on the defect segment of the framework model state diagram shown in Fig. 1 *D*. The extreme values of $\chi^d$ correspond to the boundary states at $\pm\chi_C^d$. The trajectory makes rapid excursions into the interior of the defect segment. Fig. 6 *C* shows trajectories diffusing over the defect potential profile on its entire interval of definition. The lumped state approximation is not used. Qualitatively, the appearance of Fig. 6, *B* and *C*, is somewhat similar in the region $|\chi^d| < \chi_C^d$. The mean first passage times for transport over the defect barrier are quantitatively very similar, as shown in Fig. 5 and discussed in Methods.

## Comparison with data of Eisenman et al.

Our main purpose in constructing the framework model of single-proton conduction is to compare the results of the molecular dynamics simulations (Pomès and Roux, manuscript in preparation) with experiment. Eisenman et al. (1980) summarize several studies of ion conductance through gramicidin, including an extensive investigation of proton conductance for $pH \geq 1.7$. Decker and Levitt (1988), Akeson and Deamer (1991), Phillips et al. (1999), and recently Cukierman (2000) have also made single-channel measurements in this concentration range.

Eisenman et al. provide graphs of the logarithm of conductance, $\log_{10} G_{50}$, and conductance ratio, $G_{100}/G_0$, as a function of concentration $C$, where $G_V(C)$ is the proton conductance of gramicidin A measured at symmetrical concentration $C$ and applied potential $V$. We show these data in Fig. 7, *A* and *B*. All of the data collected for $pH > 1.5$ are shown except for one outlier on each plot. To reduce clutter,

several data points with $pH < 1.5$ are omitted. The data shown here fall on or close to smooth curves drawn through the observations in the original paper.

Also shown in Fig. 7, *A* and *B*, are three fits of the framework model to the data for $pH \geq 1.7$. The data include five conductances and eight conductance ratios. Each fit is obtained by optimizing the parameters $t^a$ and $\zeta$ as described in Methods; these parameters control the entrance and exit rate of protons. The fits given by the solid and short-dashed curves use the molecular dynamics estimates of the proton and defect potentials of mean force. For the fit given by the long-dashed curves, the defect potential of mean force shown by Fig. 2 *B* was scaled by a constant factor to increase the amplitude of the central barrier by $2k_BT$. All three fits use the molecular dynamics estimates of the proton and defect diffusion coefficients, and a value of $\mu^w = 2.4$ Debye for the dipole moment of water, consistent with the results of Duca and Jordan (1997).

The fits given by the solid and long-dashed curves use the boundary regions shown in Fig. 2 *B*. We shall refer to these as the *wide* boundary regions. The fit given by the short-dashed curves uses boundary regions that are half as wide as those shown in Fig. 2 *B*. We shall refer to these as *narrow* boundary regions. Values of $\chi_A^d$, $\chi_B^d$, and $\chi_C^d$ are given in the legend of Fig. 2.

### *Conductance*

Eisenman et al. (1980) measured single-channel proton conductances in symmetrical solutions at 50 mV applied potential. These data are shown as the filled circles in Fig. 7 *A*. At the lowest concentrations, conductance is proportional to concentration, corresponding to a slope of 1 on the log-log plot. This is consistent with the idea that the proton entrance is rate limiting, which is also strongly supported by Decker and Levitt's study (1988) of the effects of weak acids on conductance at pH 2.75 and pH 3.75.

A striking feature of these data is the well-defined shoulder near pH 1.7. The existence of this shoulder has been confirmed by Akeson and Deamer (1991), and very recently a similar well-defined shoulder has been found in conductances of the RR dioxolane-linked gramicidin (Schumaker et al., 2000a; Cukierman, 2000). A formula for the framework model conductance is obtained by Schumaker et al. (2000b); its form, for the case of symmetrical concentrations and $V_I = 0$, is given by Eq. 21. Independent of the details of the potentials of mean force or diffusion coefficients, one finds that there can be no shoulder such as that displayed by the data in Fig. 7 *A*. One possible interpretation of the experimental shoulder is that it signifies the onset of significant two-proton conduction.

The quadratic dependence of the denominator of Eq. 21 on the symmetrical concentration *C* is unusual for a single-ion conduction model. At low concentrations the conductance is similar to a Langmuir isotherm; it first increases linearly with concentration and then begins to saturate. But instead of asymptotically approaching a maximum value at higher concentrations, the conductance given by Eq. 21 eventually decreases.

Physically, the decrease in conductance is due to competition between the time scales associated with defect diffusion over the central barrier of Fig. 2 *B* and proton entrance. Once a proton exits the channel in Fig. 1 *D*, a defect must diffuse over the central barrier to complete the cycle around the diagram associated with the net permeation of one proton. If a proton first reenters from the same side as the most recent exit, this cycling is frustrated. This is similar to the clogging mechanism described by Schumaker and MacKinnon (1990).

Each of the model curves shown in Fig. 7 *A* interpolates the linearly increasing conductance at high pH very well, but a difference arises in the region of the shoulder. The model curve obtained by increasing the amplitude of the defect segment central barrier is below the other two for $pH < 2$. This curve fits the data for $pH \geq 2$ well, but if the amplitude of the defect central barrier is increased much further, it is no longer possible to interpolate the data near the shoulder. This is shown by the sensitivity analysis given below. A similar comparison between model curves and the data arises if we use the defect potential of mean force obtained from molecular dynamics but decrease the defect diffusion coefficient. A good fit to the data is obtained when the defect diffusion coefficient is a factor of 4 smaller than that given by the molecular dynamics, but it becomes impossible to interpolate the shoulder if the diffusion coefficient is decreased much further.

The significance of the fits near the shoulder is not completely clear because the single-proton model does not account for the region above the shoulder. For example, if the experimental shoulder is in fact due to the onset of two-proton conductance, then this mechanism may make some contribution below the shoulder as well, but this is not taken into account here.

### *Conductance ratio*

Eisenman et al. also measured the ratio of the conductance at 100 mV to the conductance estimated near 0 mV. These conductance ratios are shown as the filled circles in Fig. 7 *B*. A ratio greater than 1 corresponds to a superlinear *I–V* curve, and a ratio less than 1 corresponds to a sublinear *I–V* curve. These data have three very interesting features: a limiting sublinear conductance ratio at high pH, an increasing conductance ratio as pH decreases to 1, and then a maximum ratio near pH 1, just above the shoulder of Fig. 7 *A*. Consistently, Cukierman has found a maximum in the conductance ratio just above the shoulder in the RR conductance data (Schumaker et al., 2000a).

The limiting ratio in the data of Eisenman et al. is significantly less than 1, corresponding to sublinear *I–V*

curves. This suggests that the rate of proton entrance is not strongly dependent on the applied potential $V_I$. As a simplifying assumption, our framework model assumes that entrance is independent of $V_I$ (Schumaker et al., 2000b). Indeed, the model *I–V* curves are also sublinear at high pH. There is, however, a difference in limiting conductance ratios between the solid and long-dashed curves, which were constructed using wide boundary regions, and the short-dashed curve, which was constructed using narrow boundary regions. The limiting ratio is larger for the narrow boundary regions. Similarly, the limiting conductance ratio depends on the assumed value $\mu^w$ of the dipole moment of a water molecule. The limiting conductance ratio increases as $\mu^w$ increases. This interplay between the width of the boundary regions and the value of $\mu^w$ is also revealed by the sensitivity analysis, which we discuss next. Each of the model fits interpolates the data well in the regime of increasing conductance ratios.

### *Sensitivity analysis*

In this section we test the sensitivity of the optimized fits of the single-proton model to the data of Eisenman et al. as we perturb the height of the defect barrier and the value of the defect diffusion coefficient obtained from molecular dynamics, and as we also perturb the assumed value of the water dipole moment, $\mu^w$. This analysis is motivated in two ways. First, the data we are fitting are limited: just five conductance data points and eight curve shape data points for pH $\geq$ 1.7. To what extent does optimization of $t^a$ and $\zeta$ give the model a general capability to interpolate these data points? Can we arbitrarily vary the potential profile and diffusion coefficients and obtain equally good fits? Second, the molecular dynamics simulations did not include a representation of the membrane or the aqueous solution on either side. Therefore, the potentials of mean force we use neglect contributions due to interactions with these components of the channel environment. If these interactions change the height of the defect potential barrier, shown in Fig. 2 *B*, this may conceivably be reflected in an improved optimized fit with the data when the height is perturbed.

To test the sensitivity of the optimized fit to the height of the defect barrier, we ran a series of analyses, using modified defect potentials of mean force. The error (the sum of the squared differences between the conductance data points and the model plus twice the sum of the squared differences between the curve shape data points and the model) was computed as a function of the change in the height of the defect potential barrier. The defect potential was rescaled to change the amplitude of the central barrier by increments of $2k_BT$. This was done for both the wide boundary regions shown in Fig. 2 *B* and for narrow boundary regions described in the legend of Fig. 2. Results are shown in Fig. 8 *A*. The height of the defect barrier can be greatly decreased, and equally good fits are obtained. However, if this height

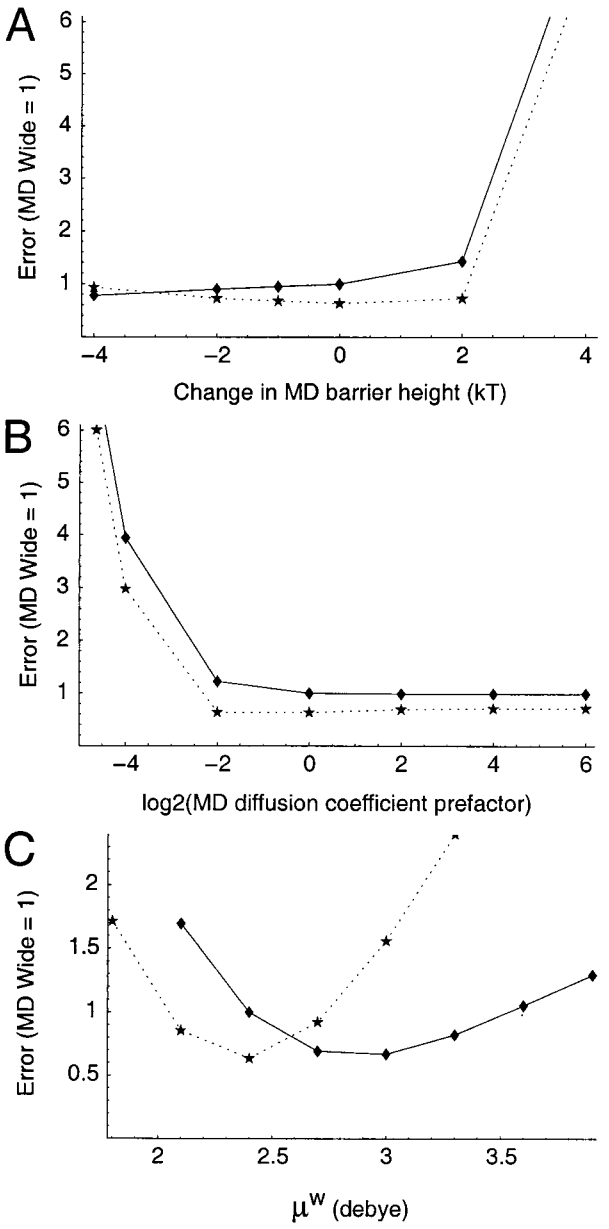


FIGURE 8 Sensitivity analysis. The error is a measure of the deviation between the model and the Eisenman conductance data for $pH \geq 1.7$ and between the model and the Eisenman curve shape data for $pH \geq 1.7$. It is scaled so that the fit using the molecular dynamics potential of mean force and diffusion coefficients with wide boundary regions and $\mu^w = 2.4$ Debye has error = 1. Diamonds connected by solid lines show the error calculated using wide boundary regions, and stars connected by dotted lines show the error calculated using narrow boundary regions. (*A*) Error as a function of change in barrier height. The amplitude of the molecular dynamics potential of mean force was rescaled to several different barrier heights. The abscissa is the difference between the rescaled barrier height and the original molecular dynamics barrier height; 0 corresponds to the molecular dynamics potential. (*B*) Error as a function of defect diffusion coefficient. The diffusion coefficient obtained from molecular dynamics is multiplied by a prefactor *p*. The abscissa is $\log_2 p$; 0 corresponds to the molecular dynamics diffusion coefficient. (*C*) Error as a function of the assumed dipole moment of water.

is increased by much more than $2k_BT$, good fits to the data are no longer possible.

To test the sensitivity of the optimized fit to the values of the defect diffusion coefficient, we also ran a series of analyses using modified diffusion coefficients. These may be expressed in the form $p\mathcal{D}^d$, where $\mathcal{D}^d$ is the result from molecular dynamics and $p$ is a prefactor. Fig. 8 *B* shows the same measure of error plotted as a function of $\log_2 p$. Results for both wide and narrow boundary regions are shown. The defect diffusion coefficient can be greatly increased beyond the value obtained from molecular dynamics, and equally good fits are obtained. However, if this diffusion coefficient is decreased by much more than a factor of 4, the fits rapidly deteriorate.

The parameter $t^a$ is inversely proportional to the proton exit rate. When either the defect diffusion coefficient is increased or the barrier height is decreased from the molecular dynamics values, the optimized values of $t^a$ vary little. These results suggest that, for these series, transport across the defect potential of mean force barrier is not rate limiting. However, when either the defect diffusion coefficient is decreased or the barrier height is increased, the optimized values of $t^a$ rapidly decrease, corresponding to a rapidly increasing optimal exit rate. Thus, for these series, the rates of proton exit and transport across the defect barrier are both important.

The proton potential of mean force, $\Phi^H$, obtained from the molecular dynamics simulations, is a shallow well. The proton diffusion coefficient, $D^H$, obtained from the Laplace transform analysis of the simulated velocity autocorrelation functions, is very high. Consequently, proton translocation through the channel is not rate limiting. Our results are insensitive to moderate changes in the proton potential profile and diffusion coefficient.

Fig. 8 *C* shows how the optimized fit varies with the assumed value of the dipole moment of water. Fits to the Eisenman et al. (1980) data set using the *narrow* boundary regions are best near $\mu^w = 2.4$ Debye, whereas fits using the *wide* boundary regions are best for $\mu^w \approx 3$ Debye. This result is somewhat surprising. The wide boundary regions, which contain the potential minima at $\chi^d = \pm 6.5\ e_0$Å, seem more reasonable than the narrow boundary regions, which are intervals of $\mu^w$ beyond the minima. However, Duca and Jordan only found values of $\mu^w$ as high as 3 Debye for waters that are nearest neighbors of a cation in the channel. A close analysis of the fits shown in Fig. 7 *B* suggests that the largest difference between the fits lies in the limiting conductance ratios at low concentrations. The conductance ratios for the wide boundary regions lie below most of the data points. This suggests a speculative explanation for the surprising result. Interfacial polarization would be expected to increase the conductance of the experimental system at low concentrations and high applied potentials (Everitt and Haydon, 1968; Walz et al., 1969), an effect that is not taken into account in our model. The biggest effect on the Eisenman data set would be to increase values of $G_{100}$ at low concentrations, increasing the experimental conductance ratio in that regime.

## Comparison with other data

Decker and Levitt (1988) have studied proton conductance through gramicidin, publishing *I–V* curves at pH 3.75 and 2.75. Fig. 7, *C* and *D*, compares their data to the fits of the three single-proton models considered in Fig. 7, *A* and *B*. The good agreement between the data and the model curves suggests that the results of Decker and Levitt are consistent with those of Eisenman et al. (1980). The data do show somewhat larger currents than the model, particularly at large $V_I$. These may well be due to small differences in experimental conditions. But the difference is also consistent with increased conductance in the experimental system due to interfacial polarization, which leads to *I–V* curves that are asymptotic to lines of positive slope at high potentials. This effect is very pronounced for $Cs^+$ conductance through gramicidin at 10 mM (Andersen, 1983).

Decker and Levitt (1988) also calculate a capture radius, $r_c$, for protons based on their data. The capture radius is defined by the formula for the flux due to diffusion toward an absorbing hemisphere of radius $r_c$. Physically this flux would correspond to a saturating current through a channel at low bulk concentration (where the current is entrance-limited) and at high applied potential (where the boundary condition at the high potential side of the membrane could be reasonably approximated as perfectly absorbing). Based on their current at 200 mV applied potential and at pH 3.75 (Fig. 7 *C*), they estimated $r_c = 0.87$ Å.

We have estimated $r_c$ by using the single-proton model formula for the saturating current in the limit of high applied potentials (Schumaker et al., 2000b). For the molecular dynamics parameter set and wide boundary regions (Fig. 7, *solid curves*) we obtain $r_c = 0.90$ Å. When the amplitude of the central barrier is increased by $2k_BT$ (*long-dashed curves*), we also obtain $r_c = 0.90$ Å. For narrow boundary regions (*short-dashed curves*) we obtain $r_c = 2.29$ Å. The higher values of $r_c$ for narrow boundary regions reflect the fact that, to fit the data, the single-proton model entrance rate must be increased to compensate as the boundary regions are made more narrow. This leads to a higher saturating current at very high applied potentials.

Akeson and Deamer (1991) have also reported single-channel measurements of proton conduction through gramicidin. Their measurements of proton currents at 59 mV as a function of pH are in qualitative agreement with the findings of Eisenman et al., including a shoulder in conductance between pH 1 and pH 2. However, they also publish an *I–V* curve at pH 2, which shows complete saturation of current as a function of voltage above $V_I = 125$ mV. The shapes of our corresponding *I–V* curves are qualitatively similar to those shown in Fig. 7, *C* and *D;* they do not have

the sharply saturating character of the data reported by Akeson and Deamer.

## SUMMARY

### Single-proton model

We summarize the construction of the single-proton conduction model. Pomès and Roux (1997) performed two sets of molecular dynamics simulations of waters in the gramicidin pore. In one set the pore includes an excess proton, and we refer to the resulting *proton* potential of mean force. This is shown in Fig. 2 *A* as a function of the orientation moment of the pore contents. It has the form of a shallow well. The molecular dynamics also estimates a diffusion coefficient for proton transport in terms of the dipole moment reaction coordinate. It is ~40 times the diffusion coefficient of protons in water, or about twice the diffusion coefficient of protons in ice.

In the second set of simulations, there is no excess proton. It is energetically favorable for the pore waters to be aligned with similar components of the dipole moment parallel to the pore axis. The alignment of the pore waters reverses when a packing defect propagates through the water chain. The corresponding *defect* potential of mean force, as a function of pore dipole moment, is shown in Fig. 2 *B*. It has a central potential barrier, $\sim 6k_BT$ high, surrounded by minima. An effective diffusion coefficient for defects is also estimated by the molecular dynamics. Its magnitude is consistent with the rate of molecular tumbling in bulk water.

The molecular dynamics simulations described above did not model proton entrance into the pore. To use these results in a theory of proton permeation through gramicidin, it is necessary to add a mechanism for proton entrance. Schumaker et al. (2000b) have developed a *framework* model of proton conduction through gramicidin. This probabilistic model is designed to incorporate the results from molecular dynamics, and includes a simple description of ion entrance and exit.

The physical assumption made by the framework model is that proton entrance is possible only when the dipole moment of the pore water column favors proton entry. This idea is illustrated by the cartoons of Fig. 1 *C*. A state diagram for the mechanism is shown in Fig. 1 *D*. The top segment of the diagram represents the set of possible proton occupied states. The bottom segment includes a continuum of states representing defect transport over the central barrier in Fig. 2 *B* and endpoints at both ends. The endpoints represent defect occupation of boundary regions near the potential minima.

The endpoints are constructed so that, in a state of symmetrical equilibrium, their probability is equal to the probability of defect occupation of the boundary regions (Schumaker et al., 2000b). We call this hybrid of discrete and continuous representations the *lumped state* approximation. The endpoints, which are the lumped states, must respond to an applied electrical field like points. As long as the boundary regions are not too wide, their effective electrical coordinate can be adjusted so that the mean first passage times to cross the central barrier using the lumped states agree closely with estimates that do not involve this approximation. This is demonstrated by the calculations used to construct Fig. 5.

The lumped state approximation makes it possible to solve the framework model analytically (Schumaker et al., 2000b). Analytical expressions for the current and conductance are found. These include dependence on the proton and defect potentials of mean force as arbitrary functions. Our model for single-proton conduction through gramicidin is the framework model combined with the results from molecular dynamics. It has three free parameters, controlling the rate of ion entrance, ion exit, and the width of the boundary regions.

### Comparison with experiment

Eisenman et al. (1980) summarized an extensive study of proton conductance in gramicidin. The data in Fig. 7, *A* and *B*, are taken from similar figures in their paper. The conductance data in Fig. 7 *A* have a well-defined shoulder for $1 < \text{pH} < 2$, with an inflection point near pH 1.7. This shoulder is impossible to fit using the single-proton model, as can be seen from the analytical formula for conductance (Eq. 21). The existence of the shoulder has been confirmed in gramicidin A by Akeson and Deamer, and a similar feature has been seen recently in the RR dioxolane dimer (Cukierman, 2000). Furthermore, a maximum in the RR curve shape ratios near $[H^+] = 100$ mM has been observed that is qualitatively similar to that seen in the data of Eisenman et al., shown in Fig. 7 *B*.

Our interpretation is that the inflection point signifies the onset of two-proton conductance, in agreement with Eisenman et al. We therefore fit the single-proton conduction model to the data in Fig. 7, *A* and *B*, only for $\text{pH} \geq 1.7$. To make the fits, we consider two values for the width of the boundary regions. The *wide* boundary regions are shown in Fig. 2 *B*, while the *narrow* boundary regions have only half the width shown. For a fixed choice of boundary regions, the two parameters controlling the proton entrance and exit rate are optimized. Good fits to the data are achieved, as shown in Fig. 7, *A* and *B*. We have studied their significance by perturbing the defect potential of mean force and diffusion coefficient. Fig. 8 *A* was constructed by repeating the optimization procedure using rescaled defect potentials with a range of barrier heights. The barrier height obtained from molecular dynamics is within a range of values that give nearly optimal fits. A similar result was found by varying the value of the defect diffusion coefficient, as shown by Fig. 8 *B*.

An important limitation of the analysis given here is that only single-proton transport through gramicidin is described, and we have no quantitative comparison with the data for pH $< 1.7$. However, we are currently extending the present model by adding rate-theory-like terms describing transitions into and out of a doubly occupied state. A good fit to the Eisenman et al. conductance data on both sides of the shoulder shown in Fig. 7 *A* can be achieved (Schumaker et al., 2000a). DeCoursey and Cherny (1999) have argued that multiple proton occupancy of the gramicidin pore is unlikely because it would require an energetically expensive defect in the hydrogen-bonded chain between the two centers of excess charge. Indeed, the shoulder in Fig. 7 *A*, between two regimes in which conductance is proportional to $[H^+]$, may be interpreted as corresponding to an increased energy barrier for ion entrance into the channel. Molecular dynamics studies would provide useful insights into the energetics of double proton occupancy and the relationship between the second proton entrance/exit process and the configuration of the hydrogen bonded chain.

Phillips et al. (1999) have recently studied proton conductance in side-chain analogs of gramicidin A channels. Fluorination of the channel $Trp^{11}$, $Trp^{13}$, or $Trp^{15}$ side chains is found to inhibit proton transport, and replacement of one or more Trps with Phe enhances transport. The observations with the fluorinated analogs were made at three proton concentrations in the range $0.018\ N \leq [H^+] \leq 0.18\ N$, and those with the Phe analogs were made at $[H^+] = 0.1$ N. They can be interpreted consistently as suggesting that increasing the electrical potential of the channel interior with respect to the membrane surface has the effect of increasing conductance. Phillips et al. explain these results by proposing that the rate-limiting step may be water reorientation mediated by an exit-initiated defect carrying a partial negative charge across the pore interior. This seems natural in view of the fact that Pomès and Roux (1997, and manuscript in preparation) found a substantial energy barrier to water reorientation (shown in Fig. 2 *B*). Increasing the electrical potential in the pore interior would lower this barrier for a negatively charged defect. Phillips et al. further argue that the dipole-dipole interaction between tryptophan and the pore waters stabilizes the orientation of waters at the side of the channel from which a proton has just exited. Then the Trp $\rightarrow$ Phe substitution should increase conductance if the creation of defects in the hydrogen-bonded chain of waters at the exit side were a rate-limiting step.

However, the simulations of Pomès and Roux (1996; manuscript in preparation) suggest that waters at either end of the pore are somewhat disordered. This disorder is associated with the minima at either end of the defect potential of mean force in Fig. 2 *B*. These results suggest that defect creation at the ends of the water chain is not rate limiting. Furthermore, there may be a difficulty with reorienting the channel waters by beginning at the end of the pore from which the proton has most recently exited. Between the two subcolumns of aligned water molecules there would be either a Bjerrum L defect with two water oxygens opposed, or a similar configuration with a water interposed between the subcolumns and making a hydrogen bond with each. Apparently, one or two of the waters in these conformations participate in only two hydrogen bonds (novel modes of hydrogen bonding may conceivably alter this conclusion; see Vargas et al., 2000). In contrast, if water reorientation begins from the other side of the pore, the defect can propagate through a series of conformations in which every water makes at least three hydrogen bonds (Pomès, 1999; Pomès and Roux, manuscript in preparation). Thus there may be an energy penalty associated with the water reorientation mechanism envisioned by Phillips et al.

The present model provides an alternative interpretation of the experimental findings of Phillips et al. In the region of the shoulder of the Eisenman conduction data, our results suggest that proton exit is a rate-limiting step. Specifically, the sensitivity analysis shows that proton exit and water reorientation rates are comparable in the shoulder region if water reorientation is somewhat slower than that calculated by the molecular dynamics (fits become impossible if water reorientation is much slower). The proton exit rate is limiting by itself in the shoulder region if water reorientation is much faster than that calculated by the molecular dynamics. Therefore, an increased electrical potential in the channel interior might plausibly speed proton exit and thus increase conductance, which is consistent with the observations. It would be very interesting to study the conductance of the side-chain analogs for a wider range of concentrations.

## APPENDIX A: ESTIMATE OF DIPOLE DIFFUSION COEFFICIENT FROM ROTATIONAL TUMBLING

A very simple estimate of the rotational diffusion coefficient of water may be developed from considerations independent of the molecular dynamics calculation. Consider Brownian motion of an overdamped degree of freedom $\mu$ with friction coefficient $\gamma$ in a harmonic potential of spring constant $K$. By equipartition, the mean value of the coordinate is given by $\langle \mu^2 \rangle = k_B T/K$. The time correlation function is

$$\langle \mu(t)\mu(0) \rangle = \langle \mu^2 \rangle \exp - t/\tau , \tag{24}$$

where $\tau = \gamma/K$ is the time constant. Its time derivative is

$$\mathrm{d}/\mathrm{d}t \langle \mu(t)\mu(0) \rangle|_{t=0} = - k_B T/\gamma = - \mathcal{D}^i , \tag{25}$$

where the Einstein relationship between friction and diffusion coefficient $\mathcal{D}^i$ is used. The pore of gramicidin contains $\sim$10 water molecules. The total dipole moment is

$$\mu = \sum_{m=1}^{10} \mu_m , \tag{26}$$

and the time correlation function is

$$\langle \mu(t)\mu(0) \rangle = \sum_{m=1}^{10} \sum_{n=1}^{10} \langle \mu_m(t)\mu_n(0) \rangle . \tag{27}$$

For the purpose of making a simple estimate, assume complete independence of the water dipoles,

$$\langle \mu_m(t)\mu_n(0)\rangle = \delta_{mn}\langle \mu_m(t)\mu_n(0)\rangle , \tag{28}$$

where $\delta_{mn} = 1$ if $m = n$ and $\delta_{mn} = 0$ otherwise. Insert this expression into Eq. 27 to obtain

$$\langle \mu(t)\mu(0)\rangle = 10\langle \mu^2\rangle e^{-t/\tau} . \tag{29}$$

Using Eq. 25, we then get

$$\mathscr{D}^i = 10\langle \mu^2\rangle/\tau . \tag{30}$$

The dipole moment of a water molecule in a gramicidin-like pore is estimated to be 0.50 $e_0$Å (Duca and Jordan, 1997), and the rotational tumbling relaxation time in bulk solution is ~7 ps at 20°C (Eisenberg and Kauzmann, 1969), giving the estimate

$$\mathscr{D}^i \approx 0.36(e_0\ \text{Å})^2(\text{ps})^{-1} . \tag{31}$$

## APPENDIX B: MFPT TO CROSS DEFECT BARRIER

In this appendix we obtain two expressions for the mean time for the defect to cross the central barrier shown in Fig. 2 *B*. Neither of these expressions assumes the lumped state approximation used by the single-proton conduction model.

### Exact mean first passage time

Calculation of mean first passage time for a diffusion process (represented by a Smoluchowski or Nernst-Planck equation) to escape a region with given boundary conditions is a standard topic in the theory of stochastic processes (Karlin and Taylor, 1981). A derivation based on the theory of random walks is given in the appendix of Schumaker and Kentler (1998). A related textbook discussion is given by Zauderer (1989).

Consider diffusion over the total defect potential $W(\mu) = \Phi^d(\mu) + \Psi^d(\mu)$, where $\Phi^d$ is the intrinsic component of the potential, pictured in Fig. 2 *B*, and $\Psi^d(\mu) = -\mu^d E$ is the component due to the applied transmembrane potential. Let $\bar{t}(\mu)$ be the mean time for a diffuser beginning at reaction coordinate $\mu = \sigma^d\chi^d$ to first reach the potential minimum at $\chi^d_{min} = 6.5\ e_0$Å, given a reflecting boundary at $-\chi^d_A = -8.1\ e_0$Å. The mean first passage time satisfies

$$D\left[\frac{\partial^2\bar{t}}{\partial\mu^2} - \frac{W'}{k_BT}\frac{\partial\bar{t}}{\partial\mu}\right] = -1 , \tag{32}$$

where $D$ is the associated diffusion coefficient and the boundary conditions are $\bar{t}'(-\mu^d_A) = 0$ and $\bar{t}(\mu^d_{min}) = 0$, where $\mu^d_{min} = \sigma^d\chi^d_{min}$. The solution may be found by the method of variation of parameters. It is

$$D\bar{t}(\mu) = \int_{-\mu^d_A}^{\mu^d_{min}} [s(\mu^d_{min}) - s(\mu')]e^{-W(\mu')/k_BT}d\mu' - \int_{-\mu^d_A}^{\mu} [s(\mu) - s(\mu')]e^{-W(\mu')/k_BT}d\mu', \tag{33}$$

with $s$ given by

$$s(\mu) = \int_{-\mu^d_A}^{\mu} e^{W(\mu')/k_BT}d\mu' . \tag{34}$$

Then $\bar{t}(-\mu^d_{min})$ is the mean first passage time to first reach the potential minimum at $\mu^d = \mu^d_{min}$, given that the trajectory starts at the potential minimum at $\mu^d = -\mu^d_{min}$ and that there is a reflecting boundary at $\mu^d = -\mu^d_A$. This is the exact mean first passage time referred to in the Methods.

### Kramers' approximation

An approximate, but simpler, expression for the rate of barrier crossing is given by Kramers' escape theory (e.g., Risken, 1989). This theory assumes that the diffuser attains a quasiequilibrium state in a deep potential well before making a transit over a high barrier. Under these conditions, transits will be nearly exponentially distributed in time. The transition rate from Kramers' theory is

$$k = D/\left(\int_{\mu_3}^{\mu_4} e^{W(\mu)/k_BT}d\mu \int_{\mu_1}^{\mu_2} e^{-W(\mu)/k_BT}d\mu\right), \tag{35}$$

and the corresponding mean first passage time is $1/k$. In this expression, the pair $\mu_1$ and $\mu_2$ span the potential minimum at $\mu_3$, and the pair $\mu_3$ and $\mu_4$ span the potential maximum. The process is absorbed at $\mu_4$. To construct Fig. 5, these integrals are evaluated numerically. When the top of the barrier and the bottom of the well can be approximated by quadratic extrema, the classical escape rate theory expression is obtained (e.g., Cooper et al., 1988; Risken, 1989).

MFS enjoyed conversations and communications with Mark Akeson, See-Wing Chiu, Sam Cukierman, Tom DeCoursey, and Eric Jakobsson, as well as the hospitality of the Departments of Chemistry and Physics at the University of Montreal, where this work began. He gratefully acknowledges the help of both Marc Souille with the computer system at the University of Montreal and of Wonpil Im with CHARMM calculations. MFS also enjoyed the hospitality extended by Brigham Young University, and particularly thanks Dr. David Busath for extensive and enjoyable conversations. He finally thanks Ann Schumaker for carefully editing the manuscript.

MFS is supported by grant MCB 9630475 from the National Science Foundation. RP is supported in part by the U.S. Department of Energy through the Los Alamos National Laboratory Directed Research and Development Grant for Bioremediation. BR is supported by the Medical Research Council of Canada.

## REFERENCES

Akeson, M., and D. W. Deamer. 1991. Proton conduction by the gramicidin water wire. *Biophys. J.* 60:101–109.

Andersen, O. S. 1983. Ion movement through gramicidin A channels. Interfacial polarization effects on single-channel current measurements. *Biophys. J.* 41:135–146.

Arseniev, A. S., I. L. Barsukov, V. F. Bystrov, A. L. Lomize, and Yu. A. Ovchinnikov. 1985. $^1$H-NMR study of gramicidin-A transmembrane ion channel: head-to-head right handed single stranded helices. *FEBS Lett.* 186:168–174.

Berne, B. J., M. Borkovec, and J. E. Sraub. 1988. Classical and modern methods in reaction rate theory. *J. Phys. Chem.* 92:3711–3725.

Berne, B. J., and R. Pecora. 1976. Dynamic Light Scattering. Wiley, New York.

Boyer, P. 1997. The ATP synthase—a splendid molecular machine. *Annu. Rev. Biochem.* 66:717–749.

Busath, D. D., C. D. Thulin, R. W. Hendershot, L. R. Phillips, P. Maughan, C. D. Cole, N. C. Bingham, S. Morrison, L. C. Baird, R. J. Hendershot, M. Cotten, and T. A. Cross. 1998. Noncontact dipole effects on channel permeation. I. Experiments with (5F-indole)$Trp^{13}$ gramicidin A channels. *Biophys. J.* 75:2830–2844.

Chang, G., R. H. Spencer, A. T. Lee, M. T. Barclay, and D. C. Rees. 1998. Structure of the MscL homolog from *Mycobacterium tuberculosis:* a gated mechanosensitive ion channel. *Science.* 282:2220–2230.

Cooper, K. E., P. Y. Gates, and R. S. Eisenberg. 1988. Diffusion theory and discrete rate constants in ion permeation. *J. Membr. Biol.* 106:95–105.

Cooper, K., E. Jakobsson, and P. Wolynes. 1985. The theory of ion transport through membrane channels. *Prog. Biophys. Mol. Biol.* 46: 51–96.

Cowan, S. W., T. Schirmer, G. Rummel, M. Steiert, R. Ghosh, R. A. Pauptit, J. N. Jansonius, and J. P. Rosenbusch. 1992. Crystal structures explain functional properties of two *E. coli* porins. *Nature.* 358:727–733.

Crouzy, S., T. B. Woolf, and B. Roux. 1994. A molecular dynamics study of gating in dioxolane linked gramicidin-A channels. *Biophys. J.* 67: 1370–1386.

Cukierman, S. 2000. Proton mobilities in water and in different stereoisomers of covalently linked gramicidin-A channels. *Biophys. J.* 78: 1825–1834.

Decker, E. R., and D. G. Levitt. 1988. Use of weak acids to determine the bulk diffusion limitation of $H^+$ ion conductance through the gramicidin channel. *Biophys. J.* 53:25–32.

DeCoursey, T. E., and V. V. Cherny. 1999. An electrophysiological comparison of voltage-gated proton channels, other ion channels, and other proton channels. *Isr. J. Chem.* 39:409–418.

Doyle, D. A., J. M. Cabral, R. A. Pfuetzner, A. Kuo, J. M. Gulbis, S. L. Cohen, B. T. Chait, and R. MacKinnon. 1998. The structure of the potassium channel: molecular basis of $K^+$ conduction and selectivity. *Science.* 280:68–76.

Duca, K. A., and P. C. Jordan. 1997. Ion-water and water-water interactions in a gramicidinlike channel: effects due to group polarizability and backbone flexibility. *Biophys. Chem.* 65:123–141.

Eisenberg, D., and W. Kauzmann. 1969. The Structure and Properties of Water. Oxford University Press, New York.

Eisenman, G., B. Enos, J. Hägglund, and J. Sandbloom. 1980. Gramicidin as an example of a single-filing ion channel. *Ann. N.Y. Acad. Sci.* 339:8–20.

Elston, T. C., and G. Oster. 1997. Protein turbines. I. The bacterial flagellar motor. *Biophys. J.* 73:703–721.

Everitt, C. T., and P. A. Haydon. 1968. Electrical capacitance of a lipid membrane separating two aqueous layers. *J. Theor. Biol.* 18:371–379.

Heinemann, S., and F. J. Sigworth. 1989. Estimation of $Na^+$ dwell time in the gramicidin A channel. $Na^+$ ions as blockers as $H^+$ currents. *Biochim. Biophys. Acta.* 987:8–14.

Hille, B. 1992. Ionic Channels of Excitable Membranes, 2nd Ed. Sinauer Associates, Sunderland, MA.

Jackson, J. D. 1975. Classical Electrodynamics. Wiley, New York.

Jordan, P. C. 1982. Electrostatic modeling of ion pores. *Biophys. J.* 39:157–164.

Jordan, P. C., R. J. Bacquet, J. A. McCammon, and P. Tran. 1989. How electrolyte shielding influences the electrical potential in transmembrane ion channels. *Biophys. J.* 55:1041–1052.

Karlin, S., and H. M. Taylor. 1981. A Second Course in Stochastic Processes. Academic Press, New York.

Ketchem, R. R., W. Hu, and T. A. Cross. 1993. High-resolution conformation of gramicidin-a in a lipid bilayer by solid state NMR. *Science.* 261:1457–1460.

Phillips, L. R., C. D. Cole, R. J. Hendershot, M. Cotten, T. A. Cross, and D. D. Busath. 1999. Non-contact dipole effects on channel permeation. III. Anomalous proton conductance effects in gramicidin. *Biophys. J.* 77:2492–2501.

Pomès, R. 1999. Theoretical studies of the Grotthus mechanism in biological proton wires. *Israel J. Chem.* 39:387–395.

Pomès, R., and B. Roux. 1996. Structure and dynamics of a proton wire: a theoretical study of $H^+$ translocation along the single file water chain in the gramicidin A channel. *Biophys. J.* 71:19–39.

Pomès, R., and B. Roux. 1997. Free energy profiles governing $H^+$ conduction in proton wires. *Biophys. J.* 72:A246.

Risken, H. 1989. The Fokker-Planck Equation. Springer-Verlag, New York.

Roux, B. 1999. Statistical mechanical equilibrium theory of selective ion channels. *Biophys. J.* 77:139–153.

Roux, B., and M. Karplus. 1993. Ion transport in the gramicidin channel: free energy of the solvated right-hand dimer in a model membrane. *J. Am. Chem. Soc.* 115:3250–3262.

Schumaker, M. F., and C. Kentler. 1998. Far-field analysis of coupled bulk and boundary layer diffusion. *Biophys. J.* 74:2235–2248.

Schumaker, M. F., and R. MacKinnon. 1990. A simple model for multi-ion permeation. *Biophys. J.* 58:975–984.

Schumaker, M. F., R. Pomès, B. Roux, and S. Cukierman. 2000a. New experimental results and an extended model of proton conduction through gramicidin. *Biophys. J.* 78:348A.

Schumaker, M. F., R. Pomès, and B. Roux. 2000b. A framework model for single proton conduction through gramicidin. *Biophys. J.* In press.

Stillinger, F. H., and C. W. David. 1978. Polarization model for water and its ion dissociation products. *J. Phys. Chem.* 69:1473–1484.

Straub, J., and B. J. Berne 1988. Molecular dynamics study of an isomerizing diatomic in a Lennard-Jones fluid. *J. Phys. Chem.* 89:4833–4847.

Vargas, R., J. Garza, D. Dixon, and P. H. Hay. 2000. How strong is the $C^{\alpha} - H\cdots 0 = C$ hydrogen bond? *J. Am. Chem. Soc.* 122:4750–4755.

Walz, D., E. Bamberg, and P. Läuger. 1969. Nonlinear electrical effects in lipid bilayer membranes. I. Ion injection. *Biophys. J.* 9:1150–1159.

Weber, T. A., and F. H. Stillinger. 1982. Reactive collisions of $H_3SO_4$ and $OH^-$ studied with the polarization model. *J. Chem. Phys.* 86: 1314–1318.

Woolf, T. B., and B. Roux. 1994. The conformational flexibility of *o*-phosphorylcholine and *o*-phosphiorylethanolamine: a molecular dynamics study of solvation effects. *J. Am. Chem. Soc.* 116:5916–5926.

Zauderer, E. 1989. Partial Differential Equations of Applied Mathematics. Wiley, New York.